Scientific Research Publishing

Journal of Applied Mathematics and Physics, 2026, 14(11), 4727-4758
https://www.scirp.org/journal/jamp
ISSN Online: 2327-4379
ISSN Print: 2327-4352

# New Method for Estimating the Zeta Potential in Microchannels from Streaming Current Data

**Leonardo S. Borges, Luciano Bedin, Fermín S. V. Bazán, Everton Boos**

Department of Mathematics, Federal University of Santa Catarina, Florianópolis, Brazil
Email: l.s.borges@ufsc.br, luciano.bedin@ufsc.br, fermin.bazan@ufsc.br, everton.boos@ufsc.br

**How to cite this paper:** Borges, L.S., Bedin, L., Bazán, F.S.V. and Boos, E. (2026) New Method for Estimating the Zeta Potential in Microchannels from Streaming Current Data. *Journal of Applied Mathematics and Physics*, **14**, 4727-4758.
https://doi.org/10.4236/jamp.2026.1411231

**Received:** May 14, 2026
**Accepted:** November 21, 2026
**Published:** November 24, 2026

Copyright © 2026 by author(s) and Scientific Research Publishing Inc.
This work is licensed under the Creative Commons Attribution International License (CC BY 4.0).
http://creativecommons.org/licenses/by/4.0/

Open Access

## Abstract

We present a novel method for estimating the zeta potential in microchannels from data on the electric streaming current induced by the pressure-driven flow of an electrolyte solution in the channel. Under the assumption of a fully developed steady-state fluid flow, the electrical potential is assumed to be governed by a boundary value problem for the Poisson-Boltzmann equation with the zeta potential acting as boundary data, which we refer to as the forward problem. The contributions of the paper include theoretical results on the well-posedness of the forward problem, as well as an iterative method that estimates the zeta potential by solving a nonlinear equation. From a practical point of view, our method requires that the forward problem be solved repeatedly and as accurately as possible, since problems of this type involve solutions with steep gradients near the plates. We achieve this by using a multidomain Chebyshev Pseudo-Spectral scheme as forward solver. To validate the effectiveness of the proposed method, numerical results obtained from data with and without noise are presented.

## Keywords

Zeta Potential, Streaming Current, Poisson-Boltzmann Equation, Inverse Problems, Chebyshev Pseudo-Spectral Methods

## 1. Introduction

Microfluidic devices have become quite important in a wide range of areas such as industrial, biomedical and environmental applications [1]-[5]. In recent years, a considerable amount of effort has been devoted to the modelling and analysis of a particular type of microfluidic system that is composed of an aqueous electrolyte solution flowing through a slit channel formed by two parallel hydrophobic plates [6]-[10]. The so-called zeta potential is defined as the electric potential very close

to the plates, at the interface of the compact and diffuse layers of the electric double layer (EDL) [9] [11]. This parameter is crucial for understanding complex electrokinetic phenomena that occur at the solid-liquid interface and that give rise to unusual liquid transport processes [1] [8] [12]. Several methods have been developed to approach the problem of estimating the zeta potential in slit channels, each of them designed to address specific tasks and to adapt to the physical constraints that arise in practical applications. For example, in [13] the inverse problem of estimating the zeta potential profile in a microchannel from velocity measurements of electroosmotic flow is approached by solving a minimization problem through the conjugate gradient method. A similar problem is studied in [9] [12] [14], where, under the assumption that steady-state velocity measurements are available, approximations for the zeta potential as a linear function of the electroosmotic velocity are obtained. Another usual technique for the determination of the zeta potential is by means of the so-called pressure-driven flow. In such a case, an aqueous electrolyte solution is forced through the microchannel under an applied hydrostatic pressure. This gives rise to an electric current in the pressure-driven flow direction, known as the electric streaming current, as well as an electrokinetic potential, referred to as the electric streaming potential [12] [15]. The streaming current measurement method to estimate the zeta potential consists of first measuring the resulting net electric streaming current in the channel and then estimating the zeta potential from suitable relationships between the given applied pressure gradient, the fluid velocity field, the measurements of the net electrical streaming current and the unknown zeta potential [7] [10] [15] [16]. Regarding the streaming potential measurement method, the procedure is analogous, except that the zeta potential is determined from the measured streaming potential along the channel. Methods based on measurements of electric streaming currents are found in [16]-[18]; for the streaming potential method, see, e.g., [12] [19]. Simultaneous determination of the zeta potential and electric surface conductivity from measurements of electric streaming current and electric streaming potential was investigated in [15] taking into account the so-called Smoluchowski equation, which states linear relationships between the unknown zeta potential, the electric surface conductivity, the gradient pressure, the measured electric streaming current and electric streaming potential. It is useful to point out that such a relationship is valid only in the case of high electrolyte concentrations or large channel heights [8] [20]. In cases of small channel heights or thick electrical double layers, the Smoluchowski equation approach is no longer valid and the coupling relationship between the zeta potential and the electric streaming current or the electric streaming potential can be very complex [6] [10]. The Smoluchowski equation approach is also no longer valid in the presence of liquid slip at the plates [7] [8] [21]-[23].

In this paper we address the inverse problem of estimating the zeta potential from data on the electric streaming current by considering a pressure-driven flow of an aqueous electrolyte solution in a slit channel formed by two hydrophobic parallel plates. Assuming a fully developed steady-state fluid flow and the zeta po-

tential at both plates being equal, the problem is approached from a 1D model. Specifically, assuming that the ionic species satisfy Boltzmann distributions, we deduce that the electric potential in the channel is governed by a nonlinear Poisson-Boltzmann equation and that the fluid velocity in the channel satisfies the steady-state Stokes equation. Furthermore, as in [8] [22] [23], we assume the presence of liquid slip at the plates, so that the fluid velocity satisfies boundary slip conditions, meaning that the tangential fluid velocity is proportional to the velocity gradient in the direction perpendicular to the plates. Our model also incorporates the effect of the surface electric charge densities of the plates on the slip length [8] [22]. Such electric contribution to the friction at the solid-liquid interface appears in connection with pressure-driven flows in microchannels with large zeta potential. Proper use of all the above assumptions together with charge neutrality conditions yields two problems: a boundary value problem for the Poisson-Boltzmann equation with the zeta potential acting as boundary data, which we refer to as the forward problem, and an integro-differential equation subject to Robin's boundary conditions for the fluid velocity.

With the model at hand, the inverse problem of estimating the zeta potential is addressed by deriving a relationship between the unknown zeta potential, a given applied pressure gradient and data on the net electric streaming current. This results in a highly nonlinear equation with the net electric streaming current flow as input and the zeta potential as root. The key point of this strategy is that the fluid velocity does not appear explicitly in the resulting equation. The novelty lies in avoiding simplifications commonly adopted in other approaches found in the literature. Behind this is the fact that our model is not restricted to particular cases, such as channels with large heights, with thin electrical double layers, low zeta potential or with constant electrical conductivity along the channel [6]. This fact suggests that the model may be useful in the case of thick, non-overlapping electrical double layers or in cases where the zeta potential is large [8].

The contributions of the paper include theoretical results on the well-posedness of the forward problem and an iterative method that estimates the zeta potential by solving a nonlinear equation. Theoretically, based on technical results regarding the nonlinear Poisson-Boltzmann equation established by the authors in [24], for microchannels with non-overlapping electric double layers, we show that the inverse problem of determining the zeta potential admits at least one solution for a wide range of values of differential pressure and electric streaming current. From a practical point of view, our method requires that the forward problem be solved repeatedly and as accurately as possible, since problems of this type involve solutions with high gradients near the plates (typical when dealing with high ionic bulk concentrations or high zeta potential). We achieve this by using a multidomain Chebyshev Pseudo-Spectral scheme as forward solver, as detailed in [24] (see also [25] [26]). Quantities defined by integrals are approximated using Clenshaw-Curtis quadrature. In summary, the search for a solution of the nonlinear equation is approached by means of a suitable mix between a fixed-point iteration

procedure and bisection method. The proposed method is tested using synthetic data with and without noise.

The paper is organized as follows. In Section 2, we describe a boundary value problem for the electric potential (the forward problem) and an auxiliary integro-differential boundary value problem for the fluid velocity that we use in formulating the inverse problem. Theoretical properties of both problems, which include the existence and uniqueness of the solution to the forward problem, are derived in Section 3. In Section 4 we present the formulation of the inverse problem together with a corresponding theoretical analysis, while in Sections 5 and 6, the practical aspects of the iterative resolution method are discussed and illustrated numerically. The paper ends with concluding remarks.

## 2. Forward Problem

Let us consider an electrolyte solution that flows through a slit microchannel formed by two hydrophobic parallel plates. We assume that the plates are close to ideal surfaces, which means that the physicochemical heterogeneities of the surface, as roughness and porosity, are supposed not to be significant [15] [20]. The liquid is forced through the microchannel under a hydrostatic pressure difference $\Delta p$ between the ends of the channel, in the longitudinal direction ($x$ direction) to the plates. This gives rise to the so-called pressure-driven flow [6] [7] [12]. We address the case where the electrolyte solution contains $M \geq 2$ ionic species. Let $q_j \neq 0$, $n_j^\infty > 0$, be the charge and the bulk ionic concentration of the $j$ th ionic species, respectively. As usual, we suppose that the charge neutrality condition

$$\sum_{j=1}^{M} q_j n_j^\infty = 0, \tag{1}$$

holds true. Denoting $e_c$ as the protonic charge, the valence of the $j$th ionic species is given by $|z_j|$, being $z_j = q_j e_c^{-1}$. Notice that, by virtue of the charge neutrality condition (1), without loss of generality, we can argue that there exists an integer $1 \leq M^* < M$ such that $q_j > 0$ for $1 \leq j \leq M^*$ and $q_j < 0$ for $M^* + 1 \leq j \leq M$.

It is well known that the pressure-driven flow of electrolyte solutions is coupled with electrokinetics effects due to the presence of the so-called *electric double layer* (EDL) [7] [10]. The EDL is composed by a compact layer of immobile ions that are strongly attracted to the solid surface and a diffuse layer which is composed by mobile ions that are less affected by electrostatic interactions. For a detailed description of the EDL and its properties, we refer the reader to [12] [27] [28]. As we are dealing with a slit microchannel, we find it suitable to assume that the length $L$ ($x$ direction) and width $w$ ($z$ direction) of the channel are much larger than its height $b$ ($y$ direction) so that, under the assumption of a laminar and fully developed flow, both the electrical double layer and the flow field can be considered as one dimensional [6] [8] [12]. The characteristic thickness of the EDL is given by the *Debye-Hückel length* [11].

$$\lambda_D = \left( \frac{\beta}{\epsilon_0 \epsilon} \sum_{j=1}^{M} q_j^2 n_j^{\infty} \right)^{-1/2}, \tag{2}$$

where $\epsilon_0$ is the vacuum permittivity, $\epsilon$ denotes the dielectric constant of the electrolyte solution and $\beta = (\kappa_B T)^{-1}$, being $\kappa_B$ the Boltzmann's constant and $T$ the equilibrium temperature of the system. As the plates are supposed to be ideal surfaces, we assume that the surface potential at each plate is constant [15]. In this work we deal only with the case where the surface potential $\zeta$ (the zeta potential) assumes the same value at each plate, *i.e.*, at $y = 0$ and $y = b$.

As the liquid is forced through the microchannel, the counter-ions in the diffuse layer of the EDL move in the opposite direction of the pressure gradient. Such direction is assumed to be the positive direction of $x$ axis. This movement results in an electric current in this direction, known as electric streaming current, and a potential difference between the two ends of the channel, called electric streaming potential [7] [12] [29] [30]. In turn, the streaming potential induces an electrical current in the opposite direction of the flow (the negative direction of $x$ axis), called the electric conduction current [10] [12] [29]. The electric conduction current drives the fluid moving in the opposite direction of the pressure gradient and gives rise to the electroviscous effect [8] [12].

Since the speed of the fluid in the channel is supposed to be slow, under steady-state and fully-developed conditions, it can be assumed that the flow field has no appreciable effects on the EDL, which means that the EDL is independent of the fluid flow [7] [12] [18]. In addition, under such conditions, it can be inferred from the Nernst-Planck model for ionic concentrations throughout the channel that the electrostatic potential in the channel can be sought in the form $\Psi(x, y) = \psi(y) + \phi(x)$. Here $\psi$ denotes the electrostatic potential in the channel considering the system in thermodynamic equilibrium and $\phi$ is the flow-induced electrostatic potential [7] [10]. Another conclusion of such analysis is that the electric potential variation in the flow direction is almost linear so that $\phi(x) = -E_x x$, where $E_x = -\frac{\partial \Psi}{\partial x}$ is the strength of the electric field. Gauss's law ensures that $\Psi$ satisfies the Poisson equation

$$\Delta \Psi = -\frac{1}{\epsilon_0 \epsilon} \rho, \tag{3}$$

where $\rho$ denotes the volumetric charge density in the channel whereas $\epsilon$ is the dielectric constant of the electrolyte. In this work, the channel height does not need to be much greater than $\lambda_D$; we only require that the two EDLs on the plates do not overlap [27] [31]. Based on this, under the additional assumption that the Boltzmann distribution is satisfied so that

$$\rho(y) = \sum_{j=1}^{M} q_j n_j^{\infty} \mathrm{e}^{-\beta q_j \psi(y)},$$

since it is required that the zeta potential be equal at $y = 0$ and $y = b$, from (3) we obtain the following boundary-value problem (BVP)

$$\begin{aligned}&\psi''(y)=-\frac{1}{\epsilon_0\epsilon}\sum_{j=1}^{M}q_j n_j^{\infty}\mathrm{e}^{-\beta q_j\psi(y)},\ 0<y<b,\\&\psi(0)=\zeta,\ \psi(b)=\zeta,\end{aligned}\tag{4}$$

which we will refer to as the forward problem in this work. Note that $\zeta$ is the boundary value of the equilibrium transverse potential $\psi$, whereas the streaming potential is the flow-induced axial potential $\phi(x)=-E_x x$; the corresponding potential difference occurs between the channel ends $x=0$ and $x=L$, not between the plates. As previously mentioned, we assume a laminar, steady-state, fully-developed fluid flow through the microchannel and such that the fluid velocity in $y$ direction is much smaller than in the $x$ direction. Then, the component $u$ of the fluid velocity along the $x$ direction depends only on the $y$ variable and satisfies the steady-state Stokes equation subject to the following slip boundary conditions [32] [33]:

$$\begin{aligned}&\eta u''(y)-p_x+\rho(y)E_x=0,\ 0<y<b,\\&\gamma_1 u'(0)=u(0),\ -\gamma_2 u'(b)=u(b).\end{aligned}\tag{5}$$

Here $\eta$ denotes the dynamic viscosity of the fluid, $p_x=\Delta p/L$ is the driving pressure differential and $\gamma_1,\gamma_2>0$ are known as slip coefficients at $y=0$ and $y=b$ respectively [7] [10] [22] [23]. The term $\rho(y)E_x$ corresponds to the electric body force generated by the flow-induced electrokinetics field [12]. As mentioned before, there are several experimental evidences indicating the presence of significant liquid slip at the plates of the microchannels [21] [23]. Besides, in the case of large zeta potentials, the electric surface charge densities of the plates contribute to the friction at the solid-liquid interface, becoming an important factor that affects the magnitude of the slip lengths [8] [22] [23]. In accordance with this observation and following [22], the slip lengths $\gamma_1,\gamma_2$ appearing in the slip boundary conditions (5) are supposed to be given by

$$\gamma_i=\frac{\gamma_0}{1+\alpha^{-1}\sigma_i^2 d^3 e_c^{-2}\ell_B\gamma_0},\ i=1,2,\tag{6}$$

where $\gamma_0>0$ is the original slip length without electric effects, $\sigma_1,\sigma_2$ are the electric surface charge densities at $y=0$ and $y=b$, respectively, $\alpha>0$ is a numerical factor, $d$ is the equilibrium distance of Lennard-Jones potential and $\ell_B=\dfrac{e_c^2\beta}{4\pi\epsilon\epsilon_0}$ is the so-called Bjerrum length of the solvent [22] [23]. Also, it holds that

$$\sigma_1=-\epsilon\epsilon_0\psi'(0),\ \sigma_2=\epsilon\epsilon_0\psi'(b).\tag{7}$$

The density of the electric current (per unit area) in the flow direction, the termed electric streaming current, is given by $J_S(y)=\rho(y)u(y)$ [7]. In turn, the electric current due to the electric streaming potential, called electric conduction current, has density (per unit area) given by $J_C(y)=\wp(y)E_x$, where

$$\wp(y)=\beta\sum_{j=1}^{M}\mu_j q_j^2 n_j^{\infty}\mathrm{e}^{-\beta q_j\psi(y)},\tag{8}$$

is the so-called electric conductivity of the electrolyte at each cross section of the channel and $\mu_j > 0$ denotes the mobility coefficient of the $j$th ionic species [6] [8] [23]. Conservation of the charge neutrality implies that the net ionic electric current must be zero over each cross section of the channel [12] [33]. This can be expressed as

$$\int_0^w \int_0^b E_x \wp(y)\,\mathrm{d}y\mathrm{d}z + \int_0^w \int_0^b \rho(y)u(y)\,\mathrm{d}y\mathrm{d}z = 0,$$

where the first and the second term above correspond, respectively, to net electric conduction current and net electric streaming current over each cross section of the channel. As a result, the electric field strength in the channel is given by

$$E_x = -\frac{\int_0^w \int_0^b \rho(y)u(y)\,\mathrm{d}y\mathrm{d}z}{\int_0^w \int_0^b \wp(y)\,\mathrm{d}y\mathrm{d}z}, \tag{9}$$

from which we see that $-E_x$ is the ratio of the net electric streaming current to the net electric conductivity of the electrolyte over each cross section of the channel. Such result was reported previously by [7] (in the dimensionless case), as well as in [6], where the electric field strength caused by the electric streaming potential is shown to be proportional to the inverse of the net electric conductivity. Of course, as $\rho$, $u$ and $\wp$ do not depend on $z$ variable, (9) takes the form

$$E_x = -\frac{\int_0^b \rho(y)u(y)\,\mathrm{d}y}{\int_0^b \wp(y)\,\mathrm{d}y}. \tag{10}$$

Thus, from (5) and (10), it follows that $u$ satisfies the following integro-differential equation subject to slip boundary conditions:

$$\eta u''(y) - p_x - \rho(y)\frac{\int_0^b \rho(\tau)u(\tau)\,\mathrm{d}\tau}{\int_0^b \wp(y)\,\mathrm{d}y} = 0,\ 0 < y < b, \tag{11}$$

$$\gamma_1 u'(0) = u(0),\ -\gamma_2 u'(b) = u(b). \tag{12}$$

The solution $u$ to (11)-(12) will be used in formulating the inverse problem of interest.

## 3. Theoretical Analysis

In this section we establish well-posedness results for the forward problem and investigate some properties of the electric potential $\psi$ and fluid velocity $u$ that will become useful in the subsequent discussion regarding the zeta potential estimation problem. Starting with the forward problem let

$$F(t) = \sum_{j=1}^{M} q_j n_j^{\infty} \mathrm{e}^{-\beta q_j t}, \tag{13}$$

so that problem (4) can be rewritten as

$$\begin{aligned} &\psi''(y) = -\frac{1}{\epsilon_0 \epsilon} F(\psi(y)),\ 0 < y < b, \\ &\psi(0) = \zeta,\ \psi(b) = \zeta. \end{aligned} \tag{14}$$

It is immediate that $F$ decreases in $\mathbb{R}$ since $F'(t) = -\beta\sum_{j=1}^{M} q_j^2 n_j^{\infty} \mathrm{e}^{-\beta q_j t} < 0, \forall t \in \mathbb{R}$. Consequently, the boundary-value problem (14) fulfils the assumptions of ([34], Theorem 3.5.2, pp. 194) (see also ([24], Theorem 1)) so that the following well-posedness result holds.

**Theorem 1.** For each $\zeta \in \mathbb{R}$ problem (14) has a unique solution $\psi(\zeta,.) \in C^2(]0,b[) \cap C^1([0,b])$. Also, the map $(\zeta, y) \in \mathbb{R} \times [0,b] \to \psi(\zeta, y)$ is continuous.

Additional properties of the electric potential $\psi$ are given below.

**Theorem 2.** The solution $\psi$ of (14) is symmetric on $[0,b]$, that is $\psi(y) = \psi(b-y)$ for all $y \in [0,b]$. Moreover, $\psi$ is increasing on $[0,b/2]$ and decreasing on $[b/2,b]$. Also, whenever $\zeta < 0$ we have

$$\zeta \le \psi(y) < 0, \ \forall y \in [0,b]. \tag{15}$$

*Proof.* Let $t = b - y$, $y \in [0,b]$, and define $\varphi(t) = \psi(b-t)$. It is easy to check that $\varphi$ also satisfies the boundary-value problem (14). The symmetric property of $\psi$ therefore follows from the uniqueness of solutions to (14). The other assertions are straightforward consequences of ([24], Theorem 3, Item 1, pp. 15). □

The mean net charge density of the ions in the electrolyte solution is given by

$$\overline{\rho} = \frac{1}{wbL}\int_0^L \int_0^w \int_0^b \rho(y)\,\mathrm{d}y\mathrm{d}z\mathrm{d}x = \frac{1}{b}\int_0^b \rho(y)\,\mathrm{d}y. \tag{16}$$

The lemma below shows that there is a close relationship between $\overline{\rho}$ and the surface charge densities at the plates.

**Lemma 3.** Let $\zeta \in \mathbb{R}$ and $\sigma_i$, $i = 1,2$, defined in (7). Then we have $\sigma_1 = \sigma_2 = -\frac{b}{2}\overline{\rho}$.

*Proof.* Integration of (4) from 0 to $b$ yields

$$\psi'(b) - \psi'(0) = -\frac{1}{\epsilon\epsilon_0}\int_0^b \rho(y)\,\mathrm{d}y,$$

*i.e.*

$$\sigma_1 + \sigma_2 = -b\overline{\rho}. \tag{17}$$

Multiplying (4) by $\psi'$ and integrating, using (7) we obtain the so-called Grahame equation

$$\sigma_2^2 - \sigma_1^2 = \frac{2\epsilon\epsilon_0}{\beta}\sum_{j=1}^{M} n_j^{\infty}\left(\mathrm{e}^{-\beta q_j \zeta} - \mathrm{e}^{-\beta q_j \zeta}\right) = 0. \tag{18}$$

Now, suppose $\zeta < 0$ and let $F$ be given by (13). Since the neutrality assumption (1) implies $F(0) = 0$, and since $F$ is decreasing on $\mathbb{R}$ and $\psi(y) < 0$ for all $y \in [0,b]$ by Theorem 2, it follows that $F(\psi(y)) > 0$ in $[0,b]$. As a result, $\overline{\rho} = b^{-1}\int_0^b F(\psi(y))\,\mathrm{d}y > 0$. Arguing analogously, $\zeta > 0$ implies $\overline{\rho} < 0$. Consequently, if $\zeta \neq 0$, by virtue of (17) and (18), we conclude that $\sigma_1 = \sigma_2 = -\frac{b}{2}\overline{\rho}$. If $\zeta = 0$, neutrality condition (1) and boundary conditions

$\psi(0)=\psi(b)=0$ ensure that $\psi=0$ is a solution of (4). By Theorem 1, such solution is unique. Accordingly, we have $\sigma_1=\sigma_2=0$ as well as $\overline{\rho}=0$ (again using (1)). □

It follows from Lemma 3 and (6) that the slip coefficients $\gamma_i$, $i=1,2$, are equal and have a common value given by

$$\gamma=\frac{\gamma_0}{1+\left(4\alpha e_c^2\right)^{-1}b^2\overline{\rho}^2d^3\ell_B\gamma_0}. \tag{19}$$

**Remark 1.** Arguing as in the proof of Lemma 3, as $\sigma=-\frac{b}{2}\overline{\rho}$, we have $\sigma>0$ if $\zeta>0$ and $\sigma<0$ if $\zeta<0$.

In what follows we discuss problem (11)-(12). First, let us introduce the mean net electric conductivity of the electrolyte in each cross section of the channel, which is given by

$$\overline{\wp}=\frac{1}{bw}\int_0^w\int_0^b\wp(y)\,\mathrm{d}y\mathrm{d}z=\frac{1}{b}\int_0^b\wp(y)\,\mathrm{d}y. \tag{20}$$

**Theorem 4.** For every $\zeta\in\mathbb{R}$, there exists at most one $u\in C^2(]0,b[)\cap C^1([0,b])$ that solves (11)-(12).

*Proof.* Suppose that $u_1,u_2\in C^2([0,b])$ are solutions of (11)-(12). Then $u:=u_1-u_2$ satisfies

$$\eta u''(y)-\frac{b\rho(y)}{\overline{\wp}}\int_0^b\rho(\tau)u(\tau)\,\mathrm{d}\tau=0,\ 0<y<b, \tag{21}$$

$$\gamma u'(0)=u(0),\ -\gamma u'(b)=u(b). \tag{22}$$

Multiplying (21) by $u$, integrating by parts, and using (12) we obtain

$$\eta\int_0^b(u')^2\,\mathrm{d}y+\eta\gamma^{-1}\left(u^2(b)+u^2(0)\right)+\frac{b}{\overline{\wp}}\left(\int_0^b\rho u\mathrm{d}y\right)^2=0. \tag{23}$$

As $\gamma>0$ and $\overline{\wp}>0$, from (23) and the smoothness of $u$ we have $u'=0$ on $[0,b]$. Hence $u(0)=u(b)=0$ so that $u\equiv0$. □

In order to obtain the solution of (11)-(12) we use (10) and integrate (11) twice to deduce that

$$u(y)=u(0)+u'(0)y+p_x\frac{y^2}{2\eta}-\frac{E_x}{\eta}G(y), \tag{24}$$

where $G(y)=\int_0^y\int_0^s\rho(\tau)\,\mathrm{d}\tau\mathrm{d}s$. Next, using (12) and (24) we see that

$$-\gamma\left(\gamma^{-1}u(0)+\frac{b}{\eta}p_x-\frac{E_x}{\eta}G'(b)\right)=\left(u(0)+\gamma^{-1}bu(0)+\frac{b^2}{2\eta}p_x-\frac{E_x}{\eta}G(b)\right),$$

implies $u(0)=K_1p_x+K_2E_x$, with $K_1=-\frac{b\gamma}{2\eta}$ and

$K_2=\frac{\gamma}{\eta(2\gamma+b)}\left[\gamma G'(b)+G(b)\right]$. From these considerations and from (24), we

get

$$u(y)=p_x\left(K_1\left(1+\gamma^{-1}y\right)+\frac{y^2}{2\eta}\right)+E_x\left(K_2\left(1+\gamma^{-1}y\right)-\frac{G(y)}{\eta}\right). \tag{25}$$

Multiplying (25) by $-\rho/\overline{\wp}$, integrating in $[0,b]$ and by using (10) we obtain

$$\begin{aligned}E_x=&-\frac{p_x}{b\overline{\wp}}\int_0^b\left(K_1\left(1+\gamma^{-1}y\right)+\frac{y^2}{2\eta}\right)\rho(y)\mathrm{d}y\\&-\frac{E_x}{b\overline{\wp}}\int_0^b\left(K_2\left(1+\gamma^{-1}y\right)-\frac{G(y)}{\eta}\right)\rho(y)\mathrm{d}y.\end{aligned} \tag{26}$$

Now, integration by parts and (4) yields

$$\int_0^b y\rho(y)\mathrm{d}y=-b\sigma, \tag{27}$$

and

$$\int_0^b y^2\rho(y)\mathrm{d}y=-b^2\sigma+2\epsilon\epsilon_0\left(b\zeta-\int_0^b\psi(y)\mathrm{d}y\right). \tag{28}$$

Analogously,

$$G(y)=\epsilon\epsilon_0\left(\zeta-\psi(y)\right)-\sigma y, \tag{29}$$

from which we get

$$G(b)=-\sigma b, \tag{30}$$

$$G'(b)=-2\sigma. \tag{31}$$

From (29), (27) and Lemma 3 we obtain

$$\begin{aligned}\int_0^b G(y)\rho(y)\mathrm{d}y&=\int_0^b\rho(y)\left(\epsilon\epsilon_0\left(\zeta-\psi(y)\right)-\sigma y\right)\mathrm{d}y\\&=-\epsilon\epsilon_0\int_0^b\rho(y)\psi(y)\mathrm{d}y-2\zeta\epsilon\epsilon_0\sigma+b\sigma^2.\end{aligned} \tag{32}$$

It follows from (30)-(31) that $K_2=-\frac{\gamma\sigma}{\eta}$. Thus, Lemma 3, (27) and (32) ensure that

$$\begin{aligned}&\int_0^b\left(K_2\left(1+\gamma^{-1}y\right)-\frac{G(y)}{\eta}\right)\rho(y)\mathrm{d}y\\&=K_2\int_0^b\rho(y)\mathrm{d}y+K_2\int_0^b\gamma^{-1}y\rho(y)\mathrm{d}y-\int_0^b\frac{G(y)}{\eta}\rho(y)\mathrm{d}y\\&=\frac{\gamma\sigma}{\eta}\left(2\sigma+b\gamma^{-1}\sigma\right)-\frac{1}{\eta}\left(-\epsilon\epsilon_0\int_0^b\rho(y)\psi(y)\mathrm{d}y-2\zeta\epsilon\epsilon_0\sigma+b\sigma^2\right).\end{aligned} \tag{33}$$

Taking inner product of (4) with $\psi$ and integrating by parts we obtain

$$\begin{aligned}\int_0^b\psi(y)\rho(y)\mathrm{d}y&=-\epsilon\epsilon_0\zeta\left(\psi'(b)-\psi'(0)\right)+\epsilon\epsilon_0\int_0^b\left[\psi'(y)\right]^2\mathrm{d}y,\\\Rightarrow\int_0^b\rho(y)\psi(y)\mathrm{d}y&=-2\zeta\sigma+\epsilon\epsilon_0\int_0^b\left[\psi'(y)\right]^2\mathrm{d}y.\end{aligned}$$

Replacing this expression in (33) we get

$$\int_0^b\left(K_2\left(1+\gamma^{-1}y\right)-\frac{G(y)}{\eta}\right)\rho(y)\mathrm{d}y=\frac{2\gamma\sigma^2}{\eta}+\frac{\epsilon^2\epsilon_0^2}{\eta}\int_0^b\left[\psi'(y)\right]^2\mathrm{d}y. \tag{34}$$

If we assume that $\zeta \neq 0$, it is readily seen that the expression in the right side of (34) is positive, as in this case it holds that $\sigma \neq 0$ (see Remark 1). Accordingly, assuming that $\zeta \neq 0$ and taking into account (26) and (34), we get

$$E_x = -\frac{\int_0^b \left( K_1\left(1+\gamma^{-1}y\right)+\frac{y^2}{2\eta}\right)\rho(y)\,\mathrm{d}y}{b\wp\overline{\varphi}+\int_0^b \left( K_2\left(1+\gamma^{-1}y\right)-\frac{G(y)}{\eta}\right)\rho(y)\,\mathrm{d}y}\,p_x. \tag{35}$$

It is not difficult to check that $u$ given by (25) with $E_x$ given by (35) satisfies (11)-(12) and that it is unique due to Theorem 4.

## 4. Inverse Problem

Having ensured the existence and uniqueness of solutions to problems (4) and (11)-(12), to describe the zeta potential inverse problem, for fixed $\zeta < 0$, consider the so-called scaled net streaming current over each cross section of the channel given by

$$I_s = \frac{1}{w}\int_0^w \int_0^b \rho(y)u(y)\,\mathrm{d}y\mathrm{d}z = \int_0^b \rho(y)u(y)\,\mathrm{d}y.$$

If $I_{\text{meas}}$ denotes the net current measured across the channel width, then the scaled current used here is $I_s = I_{\text{meas}}/w$. We will show that, using $I_s$ as input, the zeta potential can be obtained using a method for calculating roots of a non-linear equation. To make this clear, note from (9) and (35) that

$$\int_0^w \int_0^b \rho(y)u(y)\,\mathrm{d}y\mathrm{d}z = \frac{K_N}{K_D}\left(\int_0^w \int_0^b \wp(y)\,\mathrm{d}y\mathrm{d}z\right)p_x, \tag{36}$$

where

$$K_N = \int_0^b \left( K_1\left(1+\gamma^{-1}y\right)+\frac{y^2}{2\eta}\right)\rho(y)\,\mathrm{d}y, \tag{37}$$

$$K_D = b\wp\overline{\varphi}+\int_0^b \left( K_2\left(1+\gamma^{-1}y\right)-\frac{G(y)}{\eta}\right)\rho(y)\,\mathrm{d}y. \tag{38}$$

Equation (36) shows that the net electric streaming current over each cross section of the channel depends linearly on the pressure gradient, *i.e.*, we have $I_s = K_\psi \wp\overline{\varphi} b p_x$ with $K_\psi = K_N/K_D$ depending only on the potential $\psi$ (and hence on $\zeta$), which agrees with results obtained earlier in [7] [10]. The dependence of $K_\psi$ on $\zeta$ follows from Equations (27)-(32), (33), and the relation between the surface charge density of the plates and the average net charge density of the electrolyte expressed by $\sigma = -\frac{b}{2}\overline{\rho}$. Indeed, it is easily seen that

$$K_N = -\frac{b^2\gamma\overline{\rho}}{2\eta} - \frac{\epsilon\epsilon_0}{\eta}\int_0^b \psi(y)\,\mathrm{d}y + \frac{b\epsilon\epsilon_0}{\eta}\zeta, \tag{39}$$

$$K_D = b\wp\overline{\varphi} + \frac{b^2\overline{\rho}^2\gamma}{2\eta} + \frac{\epsilon\epsilon_0}{\eta}\int_0^b \rho(y)\psi(y)\,\mathrm{d}y - \frac{\epsilon\epsilon_0 b\overline{\rho}}{\eta}\zeta. \tag{40}$$

Hence since for all $\zeta < 0$ there is a unique potential $\psi$ satisfying the boundary value problem (4), see Theorem 1, we can consider maps $\zeta \in (-\infty, 0] \mapsto K_D(\zeta)$, and $\zeta \in (-\infty, 0] \mapsto K_N(\zeta)$; the same holds for other quantities that depend on $\zeta$ such as $\overline{\wp}$, $\overline{\rho}$, and $\gamma$ respectively. It is clear that all these maps are continuous.

Supposing available data on the scaled net streaming current corresponding to $\zeta = \zeta^{\#}$, $I_s^{\#}$, our approach aims to recover the zeta potential based on the highly nonlinear equation

$$K_D(\zeta) I_s^{\#} = K_N(\zeta) \overline{\wp}(\zeta) b p_x, \tag{41}$$

which follows from (36). Clearly, $\zeta^{\#}$ is a root of (41), due to (36), (39) and (40). The challenge lies in computing it efficiently. By the way, our strategy differs from usual approaches that estimate the zeta potential from measurements of the electric flow current or from measurements of the electric flow potential through the channel [16]-[18].

When the streaming current is obtained experimentally, there may not be a zeta potential associated with it. Therefore, the following question needs to be addressed: given a real number $I_s > 0$, under what conditions does the nonlinear equation

$$K_D(\zeta) I_s = K_N(\zeta) \overline{\wp}(\zeta) b p_x, \tag{42}$$

admit a root? To address this issue some technical results are required. Let $F$ be defined by

$$\mathcal{F} \doteq \mathcal{F}(I_s, p_x) = \left\{ \zeta < 0; b\overline{\wp}(\zeta) p_x + \overline{\rho}(\zeta) I_s \neq 0 \right\}.$$

The following Lemma shows that if the channel height $b$ is sufficiently large, $\mathcal{F}$ is precisely the set of all negative $\zeta$.

**Lemma 5.** Let $I_s > 0$ and $p_x < 0$ be given and suppose that there exists $\aleph > 0$ such that

$$b > \aleph \left( \frac{1}{\beta \underline{\mu} \underline{q}} \right) \left( -\frac{I_s}{p_x} \right), \tag{43}$$

where $\underline{\mu} = \min_{1 \le j \le M} \mu_j$ and $\underline{q} = \min_{1 \le j \le M} |q_j|$. Then, for all $\zeta < 0$, it holds $b\overline{\wp}(\zeta) p_x + \aleph \overline{\rho}(\zeta) I_s < 0$. In particular, if $\aleph \ge 1$, we have $\mathcal{F} = (-\infty, 0)$.

*Proof.* Suppose that $\zeta < 0$. From (8), we have

$$b\overline{\wp}(\zeta) = \beta \sum_{j=1}^{M} \mu_j q_j^2 n_j^{\infty} \int_0^b \mathrm{e}^{-\beta q_j \psi(\zeta, y)} \mathrm{d}y \ge \beta \underline{\mu} \underline{q} \sum_{j=1}^{M} |q_j| n_j^{\infty} \int_0^b \mathrm{e}^{-\beta q_j \psi(\zeta, y)} \mathrm{d}y.$$

As

$$\sum_{j=1}^{M} |q_j| n_j^{\infty} \int_0^b \mathrm{e}^{-\beta q_j \psi(\zeta, y)} \ge \sum_{j=1}^{M} q_j n_j^{\infty} \int_0^b \mathrm{e}^{-\beta q_j \psi(\zeta, y)} \mathrm{d}y = \int_0^b \rho(\zeta, y) \mathrm{d}y,$$

it holds

$$b\overline{\wp}(\zeta) \ge \beta \underline{\mu} \underline{q} b \overline{\rho}(\zeta). \tag{44}$$

Then, it follows from (43) that

$$b\overline{\wp}(\zeta)p_x \le \beta\underline{\mu}\underline{q}p_x b\overline{\rho}(\zeta) < -I_s\overline{\rho}(\zeta)\aleph,$$

which concludes the proof. □

**Remark 2.** Condition (43) with $\aleph > 1$ is typical in the case of slit channels where the channel height $b$ is on the order of micrometers. For illustration, taking parameters values usually found in the literature [7] [29], with $|q_j| \approx 10^{-19}$ C, $\beta \approx 10^{21}/\text{J}$, $p_x \approx -10^6$ Pa, $\mu_j \approx 10^{-9}$ m$^2$/s and $I_s \approx 10^{-7}$ A, we have

$$\left(\frac{1}{\beta\underline{\mu}\underline{q}}\right)\left(-\frac{I_s}{p_x}\right) \approx 10^{-6}\text{ m}.$$

On the other hand, in the case of nanochannels, the height $b$ is on the order of nanometers and inequality (43) with $\aleph > 1$ may no longer be valid. Usually, such a case is related to the EDL overlap phenomenon [27] [31], which will not be considered in this work.

The following lemma gives a lower bound for the average electric potential $\psi$ over each cross section of the channel.

**Lemma 6** Let $\lambda_D$ be given by (2). Then for each $\zeta < 0$ we have

$$2\lambda_D\zeta < \int_0^b \psi(\zeta, y)\,\mathrm{d}y < 0. \tag{45}$$

*Proof.* The right inequality follows from (15). On the other hand, from ([24], Theorem 2) we have

$$\psi(\zeta, y) \ge \zeta\frac{\sinh\left(\underline{\lambda}_D^{-1}(b-y)\right)+\sinh\left(\underline{\lambda}_D^{-1}y\right)}{\sinh\left(\underline{\lambda}_D^{-1}b\right)},\quad \forall y \in [0,b],$$

where

$$\underline{\lambda}_D = \left(\frac{\beta}{\epsilon\epsilon_0}\sum_{j=1}^{M^*} q_j^2 n_j^\infty\right)^{-1/2}. \tag{46}$$

Thus,

$$\int_0^b \psi(\zeta, y)\,\mathrm{d}y \ge \zeta\int_0^b\left(\frac{\sinh\left(\underline{\lambda}_D^{-1}(b-y)\right)+\sinh\left(\underline{\lambda}_D^{-1}y\right)}{\sinh\left(\underline{\lambda}_D^{-1}b\right)}\right)\mathrm{d}y,$$

*i.e.*,

$$\int_0^b \psi(\zeta, y)\,\mathrm{d}y \ge 2\zeta\underline{\lambda}_D\left(\frac{\cosh\left(\underline{\lambda}_D^{-1}b\right)-1}{\sinh\left(\underline{\lambda}_D^{-1}b\right)}\right).$$

It is easy to check that function $p(t) = \dfrac{\cosh\left(\underline{\lambda}_D^{-1}t\right)-1}{\sinh\left(\underline{\lambda}_D^{-1}t\right)}$ is increasing and positive for $t > 0$; also

$$\lim_{t\to 0^+} p(t) = 0,\quad \lim_{t\to+\infty} p(t) = 1.$$

We have then $0 < p(t) < 1$ for all $t > 0$, from which we conclude that

$$\int_0^b \psi(\zeta, y)\,\mathrm{d}y > 2\zeta\underline{\lambda}_D. \tag{47}$$

Inequality (45) follows from (47) and from $\lambda_D > \underline{\lambda}_D$. □

We are now in position to establish the existence of roots for (42) in the case of microchannels with non-overlapping EDL.

**Theorem 7.** Let $I_s > 0$, $p_x < 0$ such that (43) holds true with $\aleph > 1$. Also, assume that

$$\lambda_D < \frac{b}{2}\left(1 - \frac{1}{\aleph}\right). \tag{48}$$

Then (42) admits at least a root $\zeta^* < 0$.

*Proof.* Let Equation (42) be rewritten in the form $Q(\zeta) = 0$ with

$$\begin{aligned} Q(\zeta) &= 2\eta I_s b\overline{\wp}(\zeta) + I_s b^2 \overline{\rho}(\zeta)^2 \gamma(\zeta) + 2\epsilon\epsilon_0 I_s \int_0^b \rho(\zeta, y)\psi(\zeta, y)\,\mathrm{d}y \\ &\quad - 2\epsilon\epsilon_0 b\overline{\rho}(\zeta) I_s \zeta + b^3 p_x \gamma(\zeta)\overline{\rho}(\zeta)\overline{\wp}(\zeta) \\ &\quad + 2b\epsilon\epsilon_0 \overline{\wp}(\zeta) p_x \int_0^b \psi(\zeta, y)\,\mathrm{d}y - 2b^2\epsilon\epsilon_0 \overline{\wp}(\zeta) p_x \zeta, \end{aligned} \tag{49}$$

Theorem 1 ensures that $Q$ is a continuous function and that

$$Q(0) = 2\eta I_s b\overline{\wp}(0) > 0 \tag{50}$$

which follows from the fact that $\psi(0, y) = 0$ and $\rho(0, y) = 0$ because of the neutrality condition (1), uniqueness of solutions of (14), and (8). Therefore, it remains to show existence of $\bar{\zeta} < 0$ such that $Q(\bar{\zeta}) < 0$. In fact, note that due to assumptions (43) and (48) there exists a real number $\omega$ such that

$$2\lambda_D < \omega < b\left(1 - \frac{1}{\aleph}\right). \tag{51}$$

As $\gamma(\zeta) > 0$ and $\overline{\rho}(\zeta) > 0$, it follows from Lemma 5 that

$$\begin{aligned} &I_s b^2 \overline{\rho}(\zeta)^2 \gamma(\zeta) + b^3 p_x \overline{\rho}(\zeta)\overline{\wp}(\zeta) \\ &< b^2 \gamma(\zeta)\overline{\rho}(\zeta)\left(\aleph I_s \overline{\rho}(\zeta) + b p_x \overline{\wp}(\zeta)\right) < 0, \ \forall \zeta < 0. \end{aligned} \tag{52}$$

Also, as $\psi(\zeta, y) < 0$ for all $y \in [0, b]$, we have

$$2\epsilon\epsilon_0 I_s \int_0^b \rho(\zeta, y)\psi(\zeta, y)\,\mathrm{d}y < 0. \tag{53}$$

Using (45), due to (48) we have

$$\begin{aligned} &2b\epsilon\epsilon_0 \overline{\wp}(\zeta) p_x \int_0^b \psi(\zeta, y)\,\mathrm{d}y - 2b^2\epsilon\epsilon_0 \overline{\wp}(\zeta) p_x \zeta \\ &< 2b\epsilon\epsilon_0 \overline{\wp}(\zeta) p_x \zeta\left(2\lambda_D - b\right) \\ &= 2b\epsilon\epsilon_0 \overline{\wp}(\zeta) p_x \zeta\left(2\lambda_D - \omega - (b - \omega)\right) \\ &< -2b\epsilon\epsilon_0 \overline{\wp}(\zeta) p_x \zeta(b - \omega). \end{aligned} \tag{54}$$

Since (51) implies

$$0 < \frac{b}{b - \omega} < \aleph, \tag{55}$$

inequalities (52), (53) and (54) together with Lemma 5 ensure that

$$\begin{aligned} Q(\zeta) &< 2\eta I_s b\overline{\wp}(\zeta) - 2\epsilon\epsilon_0 b\overline{\rho}(\zeta) I_s\zeta - 2b\epsilon\epsilon_0\overline{\wp}(\zeta) p_x\zeta(b-\omega) \\ &< \theta_1\overline{\wp}(\zeta) + \theta_2\zeta\,\overline{\rho}(\zeta), \end{aligned} \tag{56}$$

where $\theta_1 = 2\eta I_s b$ and $\theta_2 = -2\epsilon\epsilon_0(b-\omega)\left(\frac{b}{b-\omega} - \aleph\right) I_s > 0$ due to (55). Now, according to [24, Corollary 1, pp. 6], we have

$$\varphi'(0) \geq \underline{\lambda}_D^{-1}\zeta\left[\frac{1-\cosh\left(\underline{\lambda}_D^{-1}b\right)}{\sinh\left(\underline{\lambda}_D^{-1}b\right)}\right],$$

which, together with (7) and Lemma 3, yields

$$\overline{\rho}(\zeta) = \frac{2\epsilon\epsilon_0}{b}\psi'(0) \geq \frac{2\epsilon\epsilon_0\underline{\lambda}_D^{-1}}{b}\zeta\left[\frac{1-\cosh\left(\underline{\lambda}_D^{-1}b\right)}{\sinh\left(\underline{\lambda}_D^{-1}b\right)}\right].$$

Thus,

$$\lim_{\zeta\to-\infty}\overline{\rho}(\zeta) = +\infty,$$

and it follows from (44) that

$$\lim_{\zeta\to-\infty}\overline{\wp}(\zeta) = +\infty. \tag{57}$$

Since $q_j < 0$ implies $\int_0^b \mathrm{e}^{-\beta q_j\psi(\zeta,y)}\mathrm{d}y < b$, the following holds

$$\overline{\wp}(\zeta) < \beta\overline{\mu}\left(\sum_{j=1}^{M^*} n_j^\infty q_j^2\int_0^b \mathrm{e}^{-\beta q_j\psi(\zeta,y)}\mathrm{d}y + \sum_{j=M^*+1}^{M} n_j^\infty q_j^2 b\right), \tag{58}$$

where $\overline{\mu} = \max_{1\leq j\leq M}\mu_j$; thus, by virtue of (57), we get

$$\lim_{\zeta\to-\infty}\sum_{j=1}^{M^*} n_j^\infty q_j^2\int_0^b \mathrm{e}^{-\beta q_j\psi(\zeta,y)}\mathrm{d}y = +\infty. \tag{59}$$

In addition,

$$\begin{aligned} \frac{\overline{\rho}(\zeta)}{\overline{\wp}(\zeta)} &= \frac{1}{\overline{\wp}(\zeta)}\left(\sum_{j=1}^{M^*} n_j^\infty q_j\int_0^b \mathrm{e}^{-\beta q_j\psi(\zeta,y)}\mathrm{d}y + \sum_{j=M^*+1}^{M} n_j^\infty q_j\int_0^b \mathrm{e}^{-\beta q_j\psi(\zeta,y)}\mathrm{d}y\right) \\ &> \frac{1}{\overline{\wp}(\zeta)}\left(\frac{1}{\overline{q}}\sum_{j=1}^{M^*} n_j^\infty q_j^2\int_0^b \mathrm{e}^{-\beta q_j\psi(\zeta,y)}\mathrm{d}y + \sum_{j=M^*+1}^{M} bn_j^\infty q_j\right), \end{aligned} \tag{60}$$

where $\overline{q} = \max_{1\leq j\leq M^*} q_j$. Arguing as in (58), one has

$$\frac{1}{\overline{\wp}}\sum_{j=1}^{M^*} n_j^\infty q_j^2\int_0^b \mathrm{e}^{-\beta q_j\psi(\zeta,y)}\mathrm{d}y > \frac{\delta_1}{\beta\overline{\mu}\delta_2}, \tag{61}$$

where $\delta_1$ and $\delta_2$ are given by

$$\delta_1 = \sum_{j=1}^{M^*} n_j^\infty q_j^2\int_0^b \mathrm{e}^{-\beta q_j\psi(\zeta,y)}\mathrm{d}y \quad \text{and} \tag{62}$$

$$\delta_2 = \sum_{j=1}^{M^*} n_j^\infty q_j^2\int_0^b \mathrm{e}^{-\beta q_j\psi(\zeta,y)}\mathrm{d}y + \sum_{j=M^*+1}^{M} n_j^\infty q_j^2 b. \tag{63}$$

From (59) it is clear that $\lim_{\zeta\to-\infty}\delta_1/\delta_2 = 1$, and then, in view of (61), if $|\zeta|$ is

sufficiently large, it holds

$$\frac{1}{\overline{\wp}}\sum_{j=1}^{M^*} n_j^{\infty} q_j^2 \int_0^b \mathrm{e}^{-\beta q_j \psi(\zeta,y)}\mathrm{d}y > \frac{1}{2\beta\overline{\mu}}. \tag{64}$$

Analogously, due to (57), for $|\zeta|$ sufficiently large, we have

$$\frac{z}{\overline{\wp}(\zeta)} > -\frac{1}{4\overline{q}\beta\overline{\mu}}, \text{ with } z = \sum_{j=M^*+1}^{M} b n_j^{\infty} q_j. \tag{65}$$

Therefore, from (64), (65) and (60) there exists $\xi < 0$ such that

$$\begin{aligned}\frac{\overline{\rho}(\zeta)}{\overline{\wp}(\zeta)} &= \frac{1}{\overline{\wp}(\zeta)}\left(\sum_{j=1}^{M^*} n_j^{\infty} q_j \int_0^b \mathrm{e}^{-\beta q_j \psi(\zeta,y)}\mathrm{d}y + \sum_{j=M^*+1}^{M} n_j^{\infty} q_j \int_0^b \mathrm{e}^{-\beta q_j \psi(\zeta,y)}\mathrm{d}y\right)\\ &> \frac{1}{4\overline{q}\beta\overline{\mu}},\end{aligned}$$

for all $\zeta < \xi$. Hence, taking into account (56), we get

$$Q(\zeta) < \theta_1 \overline{\wp}(\zeta) + \theta_2 \zeta\, \overline{\rho}(\zeta) = \overline{\wp}(\zeta)\left(\theta_1 + \theta_2 \zeta \frac{\overline{\rho}(\zeta)}{\overline{\wp}(\zeta)}\right) < \overline{\wp}(\zeta)\left(\theta_1 + \zeta \frac{\theta_2}{4\overline{q}\beta\overline{\mu}}\right),$$

for all $\zeta < \xi$. Consequently, if $\breve{\zeta} < \min\left\{\xi, -\frac{4\beta\overline{\mu}\overline{q}\theta_1}{\theta_2}\right\}$, we have $Q(\breve{\zeta}) < 0$, which concludes the proof. □

**Remark 3** Whenever $\aleph > 1$, assumption (48) ensures the existence of a solution to the inverse problem (42) for a wide range of values of the EDL thickness as long as the EDL is non-overlapping. This includes the important case of thick EDL, which occurs for instance if a very dilute electrolyte flows throughout the microchannel [10].

**Remark 4.** In the absence of slip at the plates (which means $\gamma_0 = 0$), $Q(\zeta) = 0$ reduces to

$$\frac{\eta}{\epsilon\epsilon_0} I_s + \frac{I_s}{b\overline{\wp}(\zeta)} \int_0^b \rho(\zeta,y)\psi(\zeta,y)\mathrm{d}y - \frac{\overline{\rho}(\zeta)}{\overline{\wp}(\zeta)} I_s \zeta = -p_x \int_0^b \psi(\zeta,y)\mathrm{d}y + b p_x \zeta. \tag{66}$$

Unlike (58) and (60), in this case we have

$$\overline{\wp}(\zeta) > \beta\underline{\mu}\underline{q}\sum_{j=1}^{M^*} n_j^{\infty} q_j \int_0^b \mathrm{e}^{-\beta q_j \psi(\zeta,y)}\mathrm{d}y, \text{ and}$$

$$\overline{\rho}(\zeta) < \sum_{j=1}^{M^*} n_j^{\infty} q_j \int_0^b \mathrm{e}^{-\beta q_j \psi(\zeta,y)}\mathrm{d}y,$$

so that

$$\left|\frac{\overline{\rho}(\zeta)}{\overline{\wp}(\zeta)} I_s \zeta\right| < \frac{I_s}{\beta\underline{\mu}\underline{q}}|\zeta|. \tag{67}$$

It follows from (15) that $\sup_{y\in[0,b]}|\psi(y)| = |\zeta|$. Then, by virtue of (67), we get

$$\left|\frac{I_s}{b\overline{\wp}(\zeta)} \int_0^b \rho(\zeta,y)\psi(\zeta,y)\mathrm{d}y\right| \le \left|\frac{\overline{\rho}(\zeta)}{\overline{\wp}(\zeta)} I_s \zeta\right| < \frac{I_s}{\beta\underline{\mu}\underline{q}}|\zeta|. \tag{68}$$

Let us assume that (43) holds true for a very large $\aleph$, that is

$$-bp_x > \aleph\left(\frac{I_s}{\beta\underline{\mu}\underline{q}}\right), \tag{69}$$

which occurs if the channel height $b$ is sufficiently large. In such a case, due to inequalities (67)-(68), many authors neglect the terms $\frac{\overline{\rho}(\zeta)}{\overline{\wp}(\zeta)} I_s\zeta$ and $\frac{I_s}{b\overline{\wp}(\zeta)}\int_0^b \rho(\zeta,y)\psi(\zeta,y)\mathrm{d}y$ in (66), as their absolute values are significantly small in comparison with the term $bp_x\zeta$ [10] [12] [15] [35]. If, in addition, the electrolyte has high bulk ionic concentrations $n_j^\infty$, the EDL is non-overlapping and the Debye-Hückel length $\lambda_D$ (and hence $\underline{\lambda}_D$) becomes quite small compared to the distance $b$ between the plates. Hence, whenever $|\zeta|$ is not too large, inequality (45) ensures that $p_x\int_0^b \psi(\zeta,y)\mathrm{d}y$ in (66) becomes so small that it can be neglected. Taking into account these remarks, Equation (66) takes the form of the well-known Smoluchowski equation

$$\frac{\eta}{\epsilon\epsilon_0} I_s = bp_x\zeta, \tag{70}$$

which gives a linear relationship between $\zeta$ and $I_s$. Equation (70) can also be obtained by means of the so-called Debye-Hückel approximation, which is valid only for sufficiently small zeta potential [6] [12]. Thus, if (70) holds true, given the pressure differential $p_x$, the zeta potential can be explicitly determined by measuring the scaled net electric streaming current $I_s$. However, cases of non-overlapping EDL appearing in connection with large zeta potential $\zeta$ have been reported in the literature [8]; in such cases, the lower bound $2\lambda_D\zeta$ cannot be neglected. This is also true if $\lambda_D$ is relatively large in comparison with $b$, which occurs if the EDL is thick [10]. Moreover, as the height $b$ of the channel becomes small, the constant $\aleph$ in (43) also becomes small and the nonlinear terms in Equation (66) cannot be ignored. Other concerns regarding the accuracy of the linear approximation (70) can be found in [6] [12] [15] [30].

To address the inverse problem of calculating the zeta potential in practice, under the assumptions of Theorem 7, we first note that the nonlinear Equation (42) can be rewritten as

$$\zeta = H(\zeta), \tag{71}$$

with

$$\begin{aligned} H(\zeta) = \Big(&2\eta I_s b\overline{\wp}(\zeta) + I_s b^2\overline{\rho}(\zeta)^2\gamma(\zeta) \\ &+ 2\epsilon\epsilon_0 I_s\int_0^b \rho(\zeta,y)\psi(\zeta,y)\mathrm{d}y + b^3 p_x\gamma(\zeta)\overline{\rho}(\zeta)\overline{\wp}(\zeta) \\ &+ 2\epsilon\epsilon_0 b\overline{\wp}(\zeta)\, p_x\int_0^b \psi(\zeta,y)\mathrm{d}y\Big)\Big(2\epsilon\epsilon_0 b\big(bp_x\overline{\wp}(\zeta) + \overline{\rho}(\zeta)I_s\big)\Big)^{-1}. \end{aligned} \tag{72}$$

Equation (71) suggests calculating the zeta potential $\zeta^*$ by using a fixed-point iteration method: given an initial guess $\zeta^{(0)} < 0$, the idea is to approximate $\zeta^*$

through the sequence

$$\zeta^{(k+1)} = H\left(\zeta^{(k)}\right),\ k \geq 0. \tag{73}$$

However, proving that $H$ is a contraction to ensure convergence of the iterations is a very difficult problem because of the many quantities involved. Aware of this, to prevent possible divergence of the iterations, we propose a numerical method that switches to an alternative strategy if iterations indicate divergence, as described in Table 1.

Although existence of a solution to the nonlinear equation is established under the assumptions of Theorem 7, uniqueness remains an open problem. Theoretically, multiple roots cannot be excluded. In practice, the proposed algorithm restricts the search to a physically admissible interval $\left[\zeta_{\min}, \zeta_{\max}\right]$, checks for a sign change before applying bisection, and can be restarted from different initial guesses. The estimated zeta potential therefore corresponds to a root found in this admissible interval, and the method does not rely on a global uniqueness claim.

Table 1. Algorithm.

**Input**: Streaming current $I_s$ and physical parameters

**Output**: $\zeta^*$ as an estimate of the sought potential $\zeta$.

**1.** Define $\zeta_{\min}$ and $\zeta_{\max}$.

**2.** Set $k = 0$ and $\zeta^{(0)}$ and choose $\zeta^{(0)} \in \left[\zeta_{\min}, \zeta_{\max}\right]$.

**3.** Evaluate $H\left(\zeta^{(k)}\right)$.

**4. If** $H\left(\zeta^{(k)}\right) \in \left[\zeta_{\min}, \zeta_{\max}\right]$ **do**

$\zeta^{(k+1)} = H\left(\zeta^{(k)}\right)$

**If** $\dfrac{\left|\zeta^{(k+1)} - \zeta^{(k)}\right|}{\left|\zeta^{(k)}\right|} < tol$ **do**

Set $\zeta^* = \zeta^{(k+1)}$ and finish.

**else do**

$k \leftarrow k+1$

Go to step 3.

**end if**

**else do**

Perform Bisection method to find $\zeta^* \in \left[\zeta_{\min}, \zeta_{\max}\right]$ and finish.

**end if**

## 5. Forward Solver

Each evaluation of $H(\zeta)$ needs the solution $\psi$ of the forward problem (14) with $\zeta$ as boundary value. One way to obtain this solution efficiently is through a multidomain Chebyshev Pseudo-Spectral method introduced in [24]. Although we can use such an approach, an aspect to consider here is that $\psi$ is symmetric with respect to the vertical line $y = b/2$, *i.e.*, $\psi(y) = \psi(b-y)$, $y \in [b/2, b]$ (see Theorem 2). Hence, since $\psi'(b/2) = 0$, instead of solving (14), to evaluate

$H(\zeta)$, we will solve

$$\begin{aligned} &\psi''(y) = -\frac{1}{\epsilon_0 \epsilon} F(\psi(y)), \ 0 < y < b, \\ &\psi'(b/2) = 0, \ \psi(b) = \zeta \end{aligned} \tag{74}$$

using the same multidomain technique mentioned above. Proceeding in this way, the solution of the BVP (14) can be obtained from the solution $\psi$ of (74) using the symmetric property $\psi(y) = \psi(b-y)$ and half the number of discretization points that would be necessary to address the problem in the entire interval. Apart from that, as in this case the BVP involves a Neumann boundary condition, for the reader's convenience, some details on the numerical treatment of the standard Chebyshev Pseudo-Spectral (CPS) method are given below.

Recall that the CPS method constructs approximate solutions as low-degree algebraic polynomials by requiring that the approximation satisfies the BVP at a specified number of points, called collocation points. In the standard CPS method the BVP is defined on $[-1,1]$ and collocation points are carefully chosen from the so-called Gauss-Lobatto nodes defined by

$$y_j = -\cos\left(\frac{\pi j}{N}\right), \ j = 0, \cdots, N. \tag{75}$$

Thus, the idea is to approximate the solution $\psi(y)$ of the BVP by a polynomial $\psi_N(y)$ that interpolates data $\left(y_j, \psi_N(y_j)\right)$ where certain $y_j$ are chosen as collocation points and where $p$th order derivatives $\psi_N^{(p)}(y_j)$ are calculated using matrix vector products. In particular, first order derivatives $\psi_N'(y_j)$ are calculated as

$$\begin{bmatrix} \psi_N'(x_0) \\ \psi_N'(x_1) \\ \vdots \\ \psi_N'(x_N) \end{bmatrix} = D \begin{bmatrix} \psi_N(x_0) \\ \psi_N(x_1) \\ \vdots \\ \psi_N(x_N) \end{bmatrix}, \tag{76}$$

where $D$ is the $(N+1)\times(N+1)$ Chebyshev differentiation matrix. High order derivatives are calculated similarly. For explicit description of the entries of $D$ as well as for approximation properties, see [36] [37].

For the problem of our interest, nodes are obtained by transforming Gauss-Lobatto nodes to the domain $[b/2, b]$ through the mapping

$$t_j = \frac{b}{4}(3 - y_j), \ j = 0, \cdots, N, \tag{77}$$

and, for simplicity, the Chebyshev differentiation matrix on the transformed domain will also be denoted by $D$. Let us also assume that matrix $D$ is partitioned into rows and columns as

$$D = \begin{bmatrix} r_0^{\mathrm{T}} \\ \vdots \\ r_N^{\mathrm{T}} \end{bmatrix} = \begin{bmatrix} d_0 & \cdots & d_N \end{bmatrix}, \ r_k, d_k \in \mathbb{R}^{N+1}.$$

Let the sought approximation to the solution $\psi$ of (74) be denoted by $\hat{\psi}$

and let $\hat{\boldsymbol{\psi}} = [\hat{\psi}_0, \cdots, \hat{\psi}_N]^{\mathrm{T}}$ with $\hat{\psi}_j = \hat{\psi}(t_j)$. Collocation points are $t_j$, $j = 0, 1, \cdots, N-1$ and CPS method requires that

$$\hat{\psi}''(t_j) = -\frac{1}{\epsilon_0 \epsilon} F\left(\hat{\psi}(t_j)\right), \quad j = 0, \cdots, N-1. \tag{78}$$

Since $\hat{\psi}$ is a $N$th degree polynomial, using (76) we have

$$\begin{bmatrix} \hat{\psi}''(t_0) \\ \vdots \\ \hat{\psi}''(t_N) \end{bmatrix} = D^2 \begin{bmatrix} \hat{\psi}(t_0) \\ \vdots \\ \hat{\psi}(t_N) \end{bmatrix} = D\left(D\hat{\boldsymbol{\psi}}\right). \tag{79}$$

To impose the boundary condition $\psi'(b/2) = 0$, we further assume that

$$D = \begin{bmatrix} r_0^{\mathrm{T}} \\ R^{\downarrow} \end{bmatrix} = \begin{bmatrix} R^{\uparrow} \\ r_{N+1}^{T} \end{bmatrix}, \quad R^{\downarrow}, R^{\uparrow} \in \mathbb{R}^{N \times (N+1)}, \tag{80}$$

with $R^{\downarrow} = \begin{bmatrix} \breve{d}_0 & \cdots & \breve{d}_N \end{bmatrix}$ and $R^{\uparrow} = \begin{bmatrix} \hat{d}_0 & \cdots & \hat{d}_N \end{bmatrix}$. Hence, since $r_0^{\mathrm{T}} \hat{\boldsymbol{\psi}} = \hat{\psi}'(b/2) = 0$, we have

$$D\hat{\boldsymbol{\psi}} = \begin{bmatrix} r_0^{\mathrm{T}} \hat{\boldsymbol{\psi}} \\ R^{\downarrow} \hat{\boldsymbol{\psi}} \end{bmatrix} = \begin{bmatrix} 0 \\ R^{\downarrow} \hat{\boldsymbol{\psi}} \end{bmatrix} = \begin{bmatrix} 0 \\ \breve{R}\hat{\psi}_* + \zeta \breve{d}_N \end{bmatrix}, \tag{81}$$

where $\hat{\psi}_* = [\hat{\psi}_0, \cdots, \hat{\psi}_{N-1}]^{\mathrm{T}}$ and $\breve{R} = \begin{bmatrix} \breve{d}_0 & \cdots & \breve{d}_{N-1} \end{bmatrix}$. Therefore, the right hand side of (79) becomes

$$\begin{aligned} D\left(D\hat{\boldsymbol{\psi}}\right) &= \begin{bmatrix} d_1 & \cdots & d_N \end{bmatrix} \left(\breve{R}\hat{\psi}_* + \zeta \breve{d}_N\right) \\ &= \begin{bmatrix} d_1 & \cdots & d_N \end{bmatrix} \breve{R}\hat{\psi}_* + \zeta \begin{bmatrix} d_1 & \cdots & d_N \end{bmatrix} \breve{d}_N. \end{aligned} \tag{82}$$

where we have used the fact that $\hat{\psi}_N = \psi(t_N) = \zeta$ due to the second boundary condition. Taking into account (82) and derivative values in (79) for $j = 0, \cdots, N-1$, we get a nonlinear system of algebraic equations with unknowns $\hat{\psi}_j, j = 0, \cdots, N-1$, given by

$$\hat{R}\breve{R}\hat{\psi}_* + \zeta \hat{R}\breve{d}_N = -\frac{1}{\epsilon_0 \epsilon} F\left(\hat{\psi}_*\right) \tag{83}$$

where $\hat{R} = \begin{bmatrix} \hat{d}_1 & \cdots & \hat{d}_N \end{bmatrix}$ and $F\left(\hat{\psi}_*\right)$ denotes a vector in $\mathbb{R}^N$ whose $j$th entry is $F\left(\hat{\psi}(t_j)\right)$.

Determining the unknowns $\hat{\psi}_j$ amounts to solving the system of nonlinear equations $\Phi(\tilde{\psi}) = 0$, where $\Phi : \mathbb{R}^N \to \mathbb{R}^N$ is given by

$$\Phi(\tilde{\psi}) = \hat{R}\breve{R}\tilde{\psi} + \zeta \hat{R}\breve{d}_N + \frac{1}{\epsilon_0 \epsilon} F(\tilde{\psi}). \tag{84}$$

which can be accomplished in many ways. In this work, we choose Newton's method since the Jacobian of $\Phi(\tilde{\psi})$, denoted by $J_\Phi(\tilde{\psi})$, is easily calculated as

$$J_\Phi(\tilde{\psi}) = \hat{R}\breve{R} + \frac{1}{\epsilon_0 \epsilon} \mathrm{diag}\left(\partial F(\tilde{\psi})/\partial \tilde{\psi}_0, \cdots, \partial F(\tilde{\psi})/\partial \tilde{\psi}_{N-1}\right). \tag{85}$$

Hence, the Newton step is given by

$$\tilde{\psi}^{(k+1)} = \tilde{\psi}^{(k)} - J_{\Phi}^{-1}\left(\tilde{\psi}^{(k)}\right)\Phi\left(\tilde{\psi}^{(k)}\right),\ k \geq 0. \tag{86}$$

We stress that the inverse in (86) should never be computed explicitly. Instead, the linear system $J_{\Phi}\left(\tilde{\psi}^{(k)}\right)w = -\Phi\left(\tilde{\psi}^{(k)}\right)$ should be solved at each iteration using direct methods such as Gaussian elimination or iterative solvers [38] [39]. With the above detailed description of the standard CPS method, the multidomain CPS-based technique can be approached without difficulties by following [24].

In our experiments, since $J_{\Phi}\left(\tilde{\psi}^{(k)}\right)$ is of small size and its condition number is low, we choose Gaussian elimination. Newton iterations stop when the relative error between two consecutive iterations is smaller than some tolerance, $\left\|\tilde{\psi}^{(k+1)} - \tilde{\psi}^{(k)}\right\|_2 \Big/ \left\|\tilde{\psi}^{(k)}\right\|_2 \leq tol$. Here we have set $tol = 10^{-6}$. We conclude the section with the observation that the calculation of $H(\zeta)$ requires, in addition to solving problem (74), the calculation of some integrals. These are calculated using Clenshaw-Curtis quadrature rule based on the same nodes as the Multidomain CPS (MCPS) method, see [37] for more details.

## 6. Numerical Experiments

To illustrate the proposed approach we will proceed to practical verification using synthetic data associated with parameters taken from the literature [7] [12]. **Table 2** contains values of the physical parameters involved in the problem that we are dealing with.

**Table 2.** Values of physical parameters.

| Name | Symbol | Value |
|---|---|---|
| Protonic charge | $e_c$ | $1.602176634\times10^{-19}$ C |
| Equilibrium temperature | $T$ | 305.15 K |
| Vacuum permittivity | $\epsilon_0$ | $8.8541878188\times10^{-12}$ F·m$^{-1}$ |
| Boltzmann's constant | $k_B$ | $1.380649\times10^{-23}$ J·K$^{-1}$ |

All computations were carried out using Matlab.

### 6.1. Case 1:1 Electrolyte

Consider a 1:1 electrolyte case, for which there are $M = 2$ ionic species with $z_1 = 1$ and $z_2 = -1$, and with $n_1^{\infty} = n_2^{\infty}$ (denoted simply as $n^{\infty}$) due to the neutrality condition (1). Thus, the forward problem (74), reads

$$\begin{aligned} &\psi''(y) = \frac{\kappa^2}{\beta e_c}\sinh\left(\beta e_c \psi(y)\right),\ 0 < y < b, \\ &\psi'(b/2) = 0,\ \psi(b) = \zeta, \end{aligned} \tag{87}$$

with $\kappa = \left(2\beta e_c^2 n^{\infty}/\epsilon_0\epsilon\right)^{1/2}$. **Table 3** summarizes parameter values used in Equa-

tion (87) and others involved in the computation of function $H$.

**Table 3.** Problem data for $M=2$ ionic species.

| Symbol | Value | Symbol | Value |
|---|---|---|---|
| $b$ | $10^{-4}$ m | $\epsilon$ | 78 |
| $p_x$ | $-10^6$ N·m$^{-3}$ | $\eta$ | $0.98\times10^{-3}$ Pa·s |
| $\gamma_0$ | $10^{-6}$ m | $\alpha$ | 0.99 |
| $d$ | $4\times10^{-10}$ m | $\mu_i$ | $7.28\times10^{-9}$ m$^2$·s$^{-1}$ |

As pointed out in [24], when the bulk ionic concentration number is large, the screening effect becomes more predominant and, as a result, the MCPS approach is more suitable to capture relevant information about the potential $\psi$. For illustration we consider problem (74) with $\zeta=-0.01$ and $\zeta=-0.3$. In each case, we used $n^\infty=10^{18}$ and $n^\infty=10^{20}$. Here we have used the MCPS approach with 3 subdomains in $[b/2,b]$, with 21 inner nodes in each subdomain. This means that at each iteration of Newton's step, a linear system of size $61\times61$ is solved. The associated potential $\psi$ is depicted in **Figure 1**.

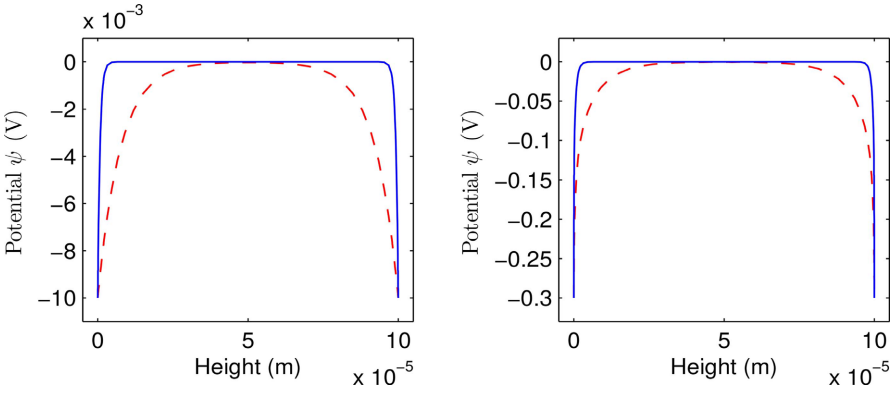


**Figure 1.** Potential $\psi$ for $\zeta=-0.01$ (left) and $\zeta=-0.3$ (right), $n^\infty=10^{18}$ (dashed line) and $n^\infty=10^{20}$ (solid line).

Before we proceed, it seems reasonable to give an example to show that our proposed scheme can, indeed, capture the desired zeta potential from a given streaming current data. To this end, let us suppose that the exact zeta potential is $\zeta=-0.2$. To construct the "exact" scaled net electric streaming current and to avoid the so-called "inverse crime", we solved the forward problem with a very large number of inner nodes in each subdomain, 201 inner nodes in each subdomain to be precise. With this, the "exact" scaled net electric streaming current is $I_s=1.616358\times10^{-5}$ (rounded to 6 decimal digits). Here $I_s$ denotes the scaled net streaming current defined in Section 4, *i.e.*, the measured net current per unit channel width. Using this $I_s$ as input data, the recovered zeta potential is $\zeta\approx-0.20000017$ which represents a relative error $\left|\zeta-(-0.2)\right|/0.2$ on the or-

der of $10^{-7}$. Although we aim to recover $\zeta = -0.2$, such a small relative error is expected due to numerical approximations.

Returning to the main goal of estimating the zeta potential from measured streaming current data, **Figure 2** depicts two examples that illustrate how $H(\zeta)$ behaves near the fixed-point $\zeta^*$, one with streaming current $I_s = 1.0\times10^{-5}$ and the other one with $I_s = 2.5\times10^{-5}$, both using $n^\infty = 10^{18}$. We shall note that values of $I_s$ and $n^\infty$ in this range are very common in the literature [7] [30].

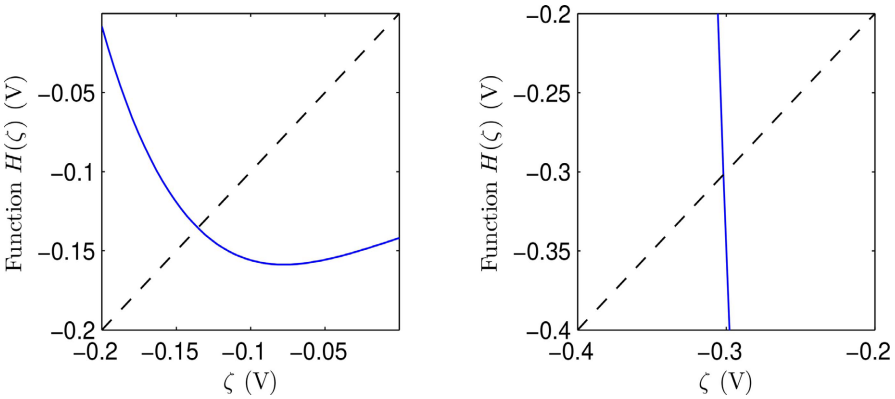


**Figure 2.** Function $H(\zeta)$ for $I_s = 1.0\times10^{-5}$ (left) and $I_s = 2.5\times10^{-5}$ (right). Both with $n^\infty = 10^{18}$. Dashed line represents the identity function.

Now we will illustrate how our proposed method works using the $I_s$ values described above. These values are interesting because, with them, both options in our algorithm are visited, once for each $I_s$. Indeed, for $I_s = 1.0\times10^{-5}$ and $\zeta^{(0)} = -0.2$ as initial guess, sequence $\zeta^{(k)}$ converges to $\zeta^* = -0.1355$ (rounded to 4 decimal digits), see **Figure 3**. The right plot of the same Figure shows consecutive relative variation of $\zeta^{(k)}$ given by

$$E_k = \left|\frac{\zeta^{(k+1)} - \zeta^{(k)}}{\zeta^{(k)}}\right|, \quad 0 \le k \le 200.$$

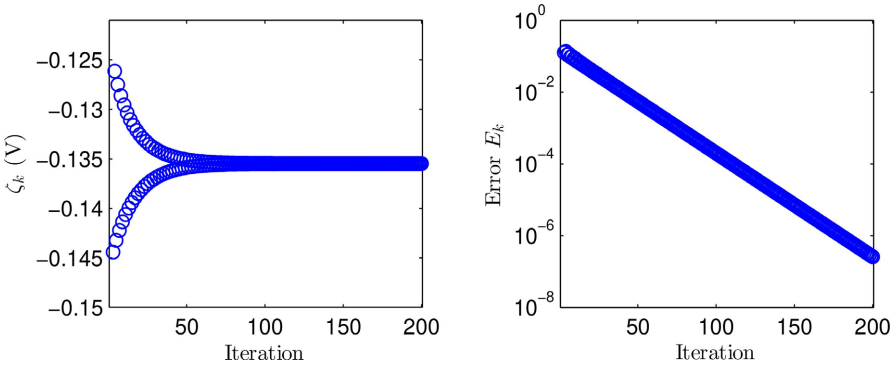


**Figure 3.** Sequence $\zeta^{(k)}$ and consecutive relative error $E_k$ for $I_s = 1.0\times10^{-5}$ and $\zeta^{(0)} = -0.2$.

In this case iterations stopped at the first $k$ such that $E_k < 10^{-6}$. However, if $I_s = 2.5\times10^{-5}$, the sequence fails to converge and our algorithm switches to the bisection method applied to the nonlinear equation $Q(\zeta) = 0$, see (49), for $\zeta \in [\zeta_{\min}, 0]$. From a physical point of view, it is very unlikely that $\zeta_{\min} < -1.0$ or even $\zeta_{\min} < -0.75$, so it seems reasonable to look for a root of $Q(\zeta)$ on the interval $[\zeta_{\min}, 0]$ with $\zeta_{\min} = -0.75$, for example. However, we learned from the proof of Theorem 7, last line, that if $\zeta < \min\left\{\xi, -\dfrac{4\beta\overline{\mu q}\theta_1}{\theta_2}\right\}$, we have $Q(\zeta) < 0$. Unfortunately, $\xi$ is not known explicitly, so we propose the following rule: set $\zeta_{\min} = \max\left\{-0.75, -\dfrac{4\beta\overline{\mu q}\theta_1}{\theta_2}\right\}$.

To summarize how our method works, we start by taking $\zeta^{(0)} \in [\zeta_{\min}, \zeta_{\max}]$ and proceed with the fixed-point sequence (73). Following the above discussion, if $\zeta^{(k+1)} \notin [\zeta_{\min}, 0]$ for some $k$, this is a strong indicative that the fixed-point iterations will not converge and the bisection method must be used instead. As an example, let us return to the problem with scaled net electric streaming current of $I_s = 2.5\times10^{-5}$, in which the fixed-point iterations failed to converge. At this point, the bisection algorithm is applied, resulting in $\zeta = -0.3019$ (rounded to 4 decimal digits) in less than 20 iterations.

Let us suppose, again, that the exact zeta potential is $\zeta = -0.2$. As mentioned before, the "exact" scaled net electric streaming current is $I_s = 1.616358\times10^{-5}$ (rounded to 6 decimal digits). To introduce noise $\varepsilon$, we consider measurements of the form $\tilde{I}_s = I_s + \varepsilon$ with relative error up to 0.1%, *i.e.*, $|\tilde{I}_s - I_s| / |I_s| \le \text{NL} = 0.001$, where NL stands for Noise Level. Considering 200 different measurements generated with Matlab's function randn, Figure 4 depicts the measured currents and the corresponding zeta potential found using the algorithm previously described. As we can see, the estimated zeta potential does not change too much from the expected value of $\zeta = -0.2$.

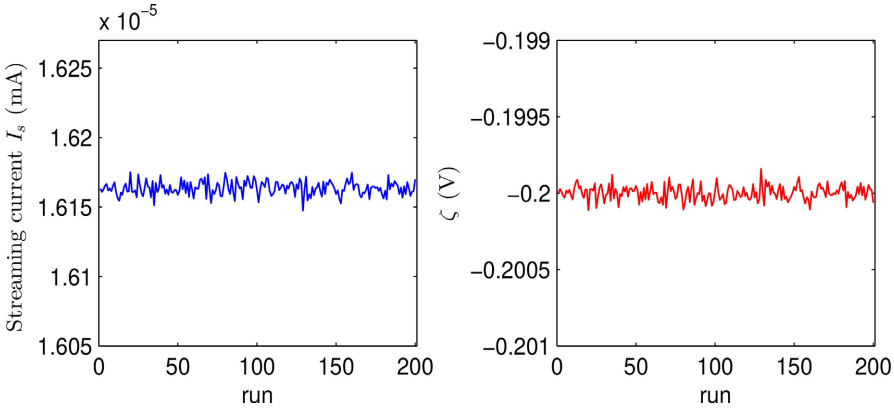


Figure 4. Measured scaled net electric streaming current (left) and corresponding zeta potential (right) for exact zeta potential $\zeta = -0.2$ and noise level up to $\text{NL} = 0.001$.

### 6.2. Case with More than 2 Ionic Species

In this example we consider an asymmetric electrolyte with $M=3$ ionic species and $z_1=1$, $z_2=2$ and $z_3=-1$. Concerning the ionic concentration, $n_1^\infty$ and $n_2^\infty$ can be freely chosen but, due to neutrality condition, $n_3^\infty$ must satisfy $n_3^\infty=n_1^\infty+2n_2^\infty$. Hence, Equation (4) can be read as

$$\psi''(y)=\frac{\kappa_1^2}{\beta e_c}\sinh\left(\beta e_c\psi(y)\right)-\frac{\kappa_2^2}{\beta e_c}\left(\mathrm{e}^{-2\beta e_c\psi(y)}-\mathrm{e}^{\beta e_c\psi(y)}\right),\ 0<y<b, \tag{88}$$

with $\kappa_1=\left(\frac{2\beta e_c^2 n_1^\infty}{\epsilon_0\epsilon}\right)^{1/2}$ and $\kappa_2=\left(\frac{2\beta e_c^2 n_2^\infty}{\epsilon_0\epsilon}\right)^{1/2}$. The boundary conditions are the same, *i.e.*, $\psi(0)=\psi(b)=\zeta$.

As before, we can exploit the fact that the solution is symmetric with respect to the line $y=b/2$. The discretization using CPS/MCPS is analogous to the case $M=2$, therefore, there is no need for further clarification and only the obtained numerical results shall be discussed.

Using the same values displayed in Table 3, Figure 5 depicts the potential $\psi$ for $\zeta=-0.01$ (left) and $\zeta=-0.3$ (right). Concerning the ionic concentration, we have $n_1^\infty=n_2^\infty=10^{18}$ (dashed line) and $n_1^\infty=n_2^\infty=10^{20}$ (solid line). In each combination ($\zeta$, $n_1^\infty$ and $n_2^\infty$), 3 subdomains in $[b/2,b]$ and 21 inner nodes per subdomain were used. As expected, with high ionic concentration, the screening effect becomes more prominent near the plates.

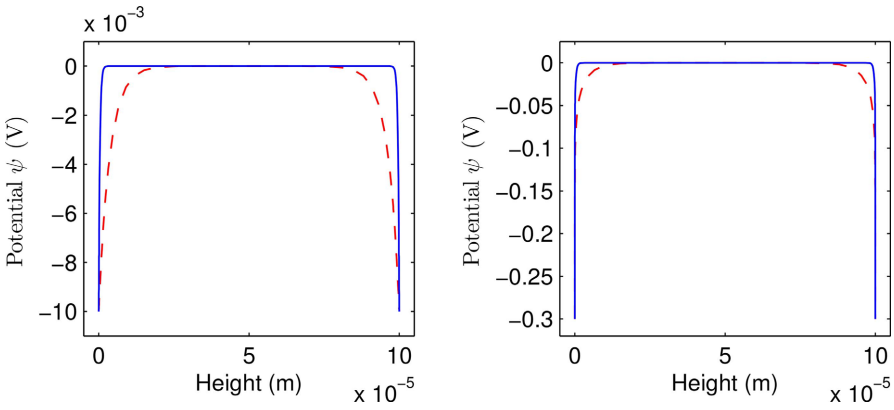


**Figure 5.** Potential $\psi$ for $\zeta=-0.01$ (left) and $\zeta=-0.3$ (right), for $n^\infty=10^{18}$ (dashed line) and $n^\infty=10^{20}$ (solid line).

There is no reason to expect that the behaviour of function $H$ will change when using $M=3$. Figure 6 illustrates, for $n_1^\infty=n_2^\infty=10^{18}$, the exact same situation as shown in the case with $M=2$. When the scaled net electric streaming current is $I_s=0.5\times10^{-5}$ (left), it is expected that the fixed-point iterations (73) may converge (depending on the initial guess $\zeta^{(0)}$). However, it may diverge when $I_s=1.0\times10^{-5}$ (right), since the derivative of $H$ near the fixed-point is greater than 1 (in absolute value).

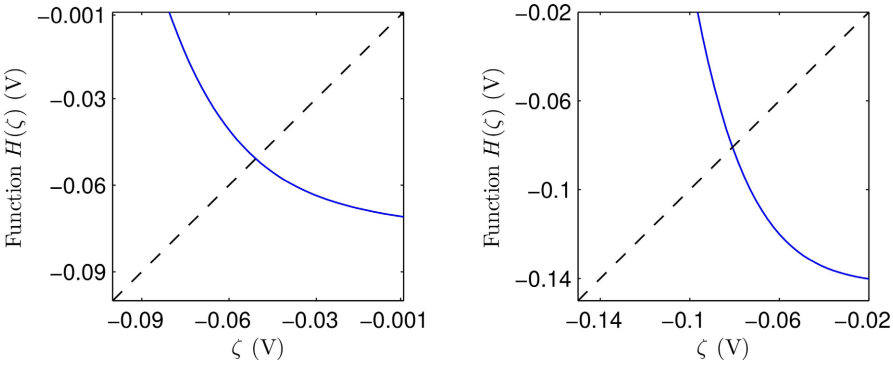


**Figure 6.** Function $H(\zeta)$ for $I_s = 0.5\times10^{-5}$ (left) and $I_s = 1.0\times10^{-5}$ (right). Both with $n^{\infty} = 10^{18}$. Dashed line is the identity function.

Since it is expected that the iterations (73) should converge when the scaled net electric streaming current is $I_s = 0.5\times10^{-5}$, let us see how such sequence behaves. For an initial guess of $\zeta^{(0)} = -0.01$, it is clear that in just a few iterations the values of $\zeta^{(k)}$ quickly stagnate, as it can be seen in the left plot of **Figure 7**. The relative error (right plot) decreases as well. Nevertheless, 131 iterations were needed to reach $E_k < tol$ with $tol = 10^{-6}$ and $\zeta^{*} = -0.05081$ (rounded to 5 decimal digits).

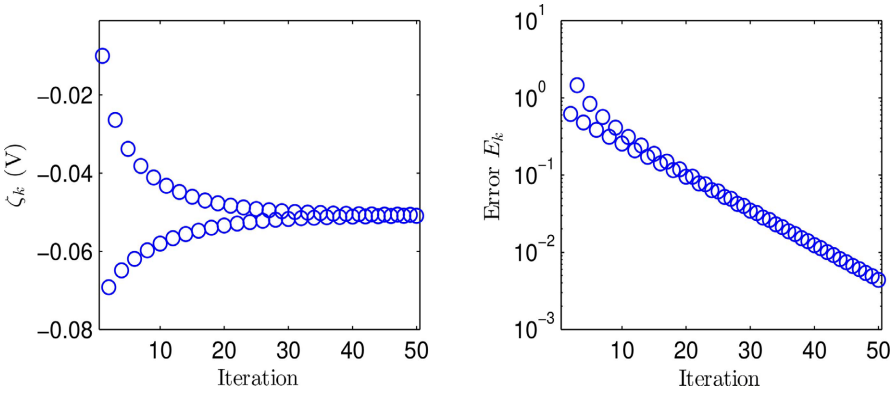


**Figure 7.** Sequence $\zeta^{(k)}$ and consecutive relative error $E_k$ for $I_s = 0.5\times10^{-5}$ and $\zeta^{(0)} = -0.01$.

Finally, to simulate noise, we proceed in the same way as before. As expected, the estimated zeta potential does not change drastically if the measured scaled net electric streaming current is contaminated with noise. For a zeta potential of $\zeta = -0.1$, the "exact" scaled net electric streaming current is $I_s = 1.506147\times10^{-5}$ (rounded to 6 decimal digits). **Figure 8** shows values obtained in 200 different measures of $\tilde{I}_s$, and, again, Noise Level is up to 0.1%. This means that $\left|\tilde{I}_s - I_s\right| / \left|I_s\right| \le 0.001$. As before, the values of the estimated zeta potential do not change much if the measured scaled net electric streaming current is contaminated with noise.

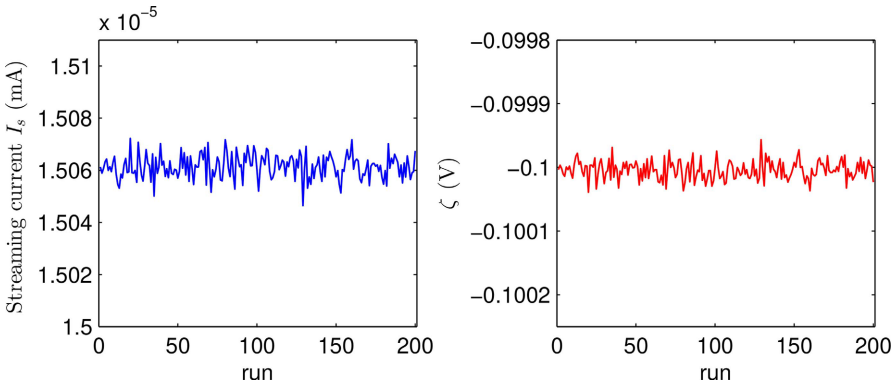


**Figure 8.** Measured scaled net electric streaming current (left) and corresponding zeta potential (right) for exact zeta potential $\zeta = -0.1$ and noise level up to $\mathrm{NL} = 0.001$.

### 6.3. Low Scaled Net Electric Streaming Current

In practical applications it is very common to have a low value for the scaled net electric streaming current $I_s$. As our last example, we will consider the case with $I_s = 10^{-8}$. **Figure 9** depicts function $H(\zeta)$ for medium/low bulk ionic concentration ($n^\infty = 5\times 10^{16}$ -left plot) and for high bulk ionic concentration ($n^\infty = 10^{18}$ - right plot). The case where $n^\infty = 5\times 10^{16}$ is particularly interesting, because the Debye-Hückel length $\lambda_D$ given by (2), which characterize the thickness of the EDL, is large in comparison with the channel height $b$. This means that we are addressing the case of a thick EDL, where the simplifications described in Remark 4 are no longer valid and our nonlinear approach becomes essential. Although $\lambda_D$ is relatively large, as we are assuming that $I_s$ is low, it is not difficult to check that the conditions (43) and (48) hold true for some $\aleph > 1$. In summary, we are dealing with a thick non-overlapping EDL.

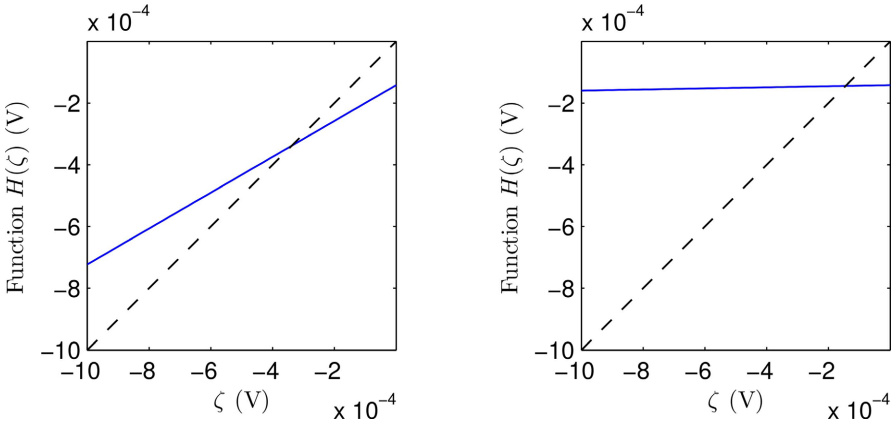


**Figure 9.** Function $H(\zeta)$ for $I_s = 10^{-8}$ with $n^\infty = 5\times 10^{16}$ (left) and $n^\infty = 10^{18}$ (right). Dashed line is the identity function.

For the fixed-point iterations, let us define $\zeta^{(0)} = -0.01$ as initial guess. In this case, with just a few iterations, a good value for the fixed-point is rapidly found, as we can see in **Figure 10**.

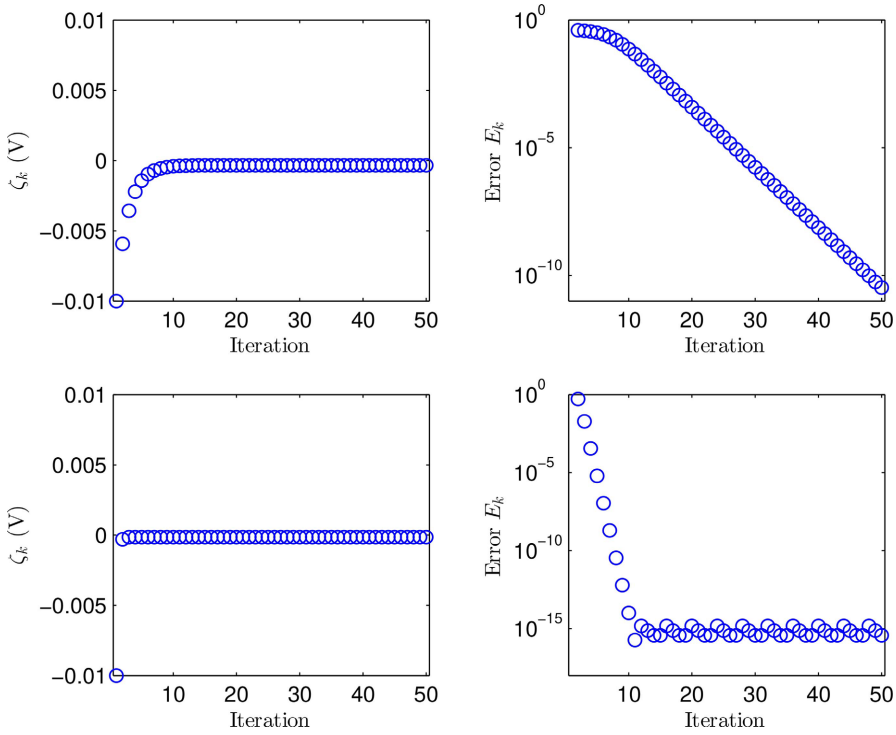


**Figure 10.** Sequence $\zeta^{(k)}$ and consecutive relative error $E_k$ for $I_s = 10^{-8}$ with $n^{\infty} = 5\times10^{16}$ (first row) and with $n^{\infty} = 10^{18}$ (second row).

To simulate noise, as we did in previous examples, for a zeta potential of $\zeta = -0.01$, the "exact" scaled net electric streaming current is $I_s = 6.923641\times10^{-7}$ (rounded to 6 decimal digits). **Figure 11** shows values obtained in 200 different measures of $\tilde{I}_s$ and, again, Noise Level is up to 0.1%. As before, the values of the estimated zeta potential do not change substantially.

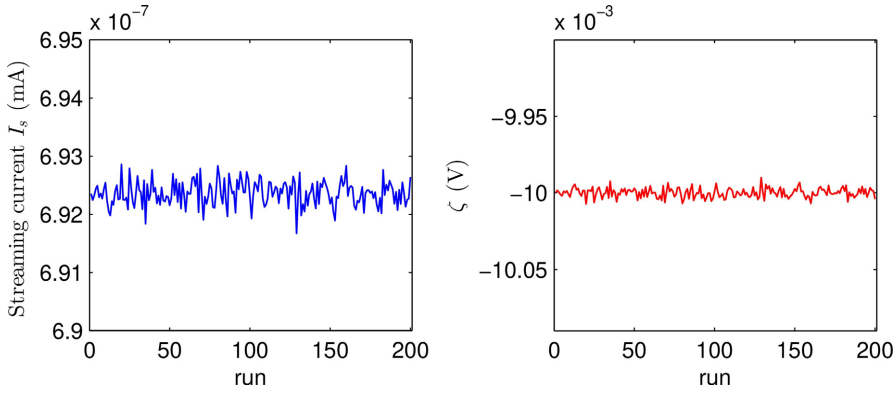


**Figure 11.** Measured scaled net electric streaming current (left) and corresponding zeta potential (right) for exact zeta potential $\zeta = -0.01$ and noise level up to NL = 0.001.

## 7. Conclusion

The current work considers the problem of estimating the zeta potential from net

electric streaming current measurements in microchannels with non-overlapping electric double layers. We start by providing a comprehensive theoretical analysis that proved well-posedness for the forward problem and existence of solutions for the inverse problem under typical conditions of non-overlapping EDLs, including cases with large zeta potentials or thick EDLs. Uniqueness remains an open problem, although numerical experiments strongly suggest it holds. These results provide a foundation for practical applications in microfluidics, particularly for systems with hydrophobic surfaces and slip boundary conditions. An important contribution is obtained when the inverse problem is reformulated as a fixed-point equation, for which a numerical method is developed. To efficiently solve the Poisson-Boltzmann equation in the forward problem at each iteration, a discretization focused on the multidomain Chebyshev Pseudo-Spectral method was essential. This technique provided a low-cost numerical approach, in the meantime accurately dealing with high gradient variations of the solution near the plates caused by large bulk ionic concentration numbers. In sequence, our proposal for the inverse problem solution combines natural fixed-point iterations and the bisection method, the last chosen to handle non-convergent scenarios. Numerical experiments with symmetric and asymmetric electrolytes confirmed that the method is accurate and stable even under noise on the electric streaming current data, fundamental in real-life applications. The proposed method is applicable under equal wall zeta potentials, one-dimensional fully developed steady flow, non-overlapping electric double layers, and negative zeta potentials in the inverse analysis. Future work may extend the ideas to overlapping EDLs, nanochannels, or experimental validation with real microfluidic devices.

## Acknowledgements

This work was supported by the "Fundação de Amparo à Pesquisa e Inovação do Estado de Santa Catarina (FAPESC)", calls for proposals 21/2024, grant 2024TR002238.

## Author Contributions

Conceptualization, L. S. Borges and L. Bedin; methodology, L. S. Borges, L. Bedin, F. S. V. Bazán and E. Boos; software, L. S. Borges; validation, L. S. Borges and E. Boos; formal analysis, L. Bedin; investigation, L. Bedin and F. S. V. Bazán; data curation, L. S. Borges; writing original draft preparation, L. S. Borges, L. Bedin, F. S. V. Bazán and E. Boos; writing review and editing, E. Boos. All authors have read and agreed to the published version of the manuscript.

## Conflicts of Interest

The authors declare no conflicts of interest regarding the publication of this paper.

## References

[1] Cho, D., Lee, S.G. and Frey, M.W. (2012) Characterizing Zeta Potential of Functional

Nanofibers in a Microfluidic Device. *Journal of Colloid and Interface Science*, **372**, 252-260. https://doi.org/10.1016/j.jcis.2012.01.007

[2] Fan, B., Bhattacharya, A. and Bandaru, P.R. (2018) Enhanced Voltage Generation through Electrolyte Flow on Liquid-Filled Surfaces. *Nature Communications*, **9**, Article No. 4050. https://doi.org/10.1038/s41467-018-06297-9

[3] Figeys, D. and Pinto, D. (2000) Lab-on-a-Chip: A Revolution in Biological and Medical Sciences. *Analytical Chemistry*, **72**, 330 A-335 A. https://doi.org/10.1021/ac002800y

[4] Squires, T.M. and Quake, S.R. (2005) Microfluidics: Fluid Physics at the Nanoliter Scale. *Reviews of Modern Physics*, **77**, 977-1026. https://doi.org/10.1103/revmodphys.77.977

[5] Verschueren, A.R.M., Notten, P.H.L., Schlangen, L.J.M., Strubbe, F., Beunis, F. and Neyts, K. (2008) Screening and Separation of Charges in Microscale Devices: Complete Planar Solution of the Poisson-Boltzmann Equation. *The Journal of Physical Chemistry B*, **112**, 13038-13050. https://doi.org/10.1021/jp800675w

[6] Ban, H., Lin, B. and Song, Z. (2010) Effect of Electrical Double Layer on Electric Conductivity and Pressure Drop in a Pressure-Driven Microchannel Flow. *Biomicrofluidics*, **4**, Article ID: 014104. https://doi.org/10.1063/1.3328091

[7] Jamaati, J., Niazmand, H. and Renksizbulut, M. (2010) Pressure-Driven Electrokinetic Slip-Flow in Planar Microchannels. *International Journal of Thermal Sciences*, **49**, 1165-1174. https://doi.org/10.1016/j.ijthermalsci.2010.01.008

[8] Jing, D. and Bhushan, B. (2015) Electroviscous Effect on Fluid Drag in a Microchannel with Large Zeta Potential. *Beilstein Journal of Nanotechnology*, **6**, 2207-2216. https://doi.org/10.3762/bjnano.6.226

[9] Lin, C.H. and Chaudhury, M.K. (2008) Using Electrocapillarity to Measure the Zeta Potential of a Planar Hydrophobic Surface in Contact with Water and Nonionic Surfactant Solutions. *Langmuir*, **24**, 14276-14281. https://doi.org/10.1021/la8027572

[10] Mirbozorgi, S.A., Niazmand, H. and Renksizbulut, M. (2007) Streaming Electric Potential in Pressure-Driven Flows through Reservoir-Connected Microchannels. *Journal of Fluids Engineering*, **129**, 1346-1357. https://doi.org/10.1115/1.2776967

[11] Israelachvili, J.N. (2011) Intermolecular and Surface Forces. 3rd Edition, Academic Press.

[12] Li, D. (2004) Electrokinetics in Microfluidics. Interface Science and Technology Series, Vol. 2, Elsevier.

[13] Park, H.M. and Choi, Y.J. (2007) Estimation of Inhomogeneous Zeta Potential in the Electroosmotic Flow Using a Moving Sensor. *Colloids and Surfaces A*: *Physicochemical and Engineering Aspects*, **307**, 93-99. https://doi.org/10.1016/j.colsurfa.2007.05.005

[14] Inagawa, A., Fukuyama, M., Hibara, A., Harada, M. and Okada, T. (2018) Zeta Potential Determination with a Microchannel Fabricated in Solidified Solvents. *Journal of Colloid and Interface Science*, **532**, 231-235. https://doi.org/10.1016/j.jcis.2018.07.137

[15] Werner, C., Zimmermann, R. and Kratzmüller, T. (2001) Streaming Potential and Streaming Current Measurements at Planar Solid/Liquid Interfaces for Simultaneous Determination of Zeta Potential and Surface Conductivity. *Colloids and Surfaces A*: *Physicochemical and Engineering Aspects*, **192**, 205-213. https://doi.org/10.1016/s0927-7757(01)00725-7

[16] Renaud, L., Kleimann, P. and Morin, P. (2004) Zeta Potential Determination by

Streaming Current Modelization and Measurement in Electrophoretic Microfluidic Systems. *Electrophoresis*, **25**, 123-127. https://doi.org/10.1002/elps.200305696

[17] Lenzi, A., Viola, F., Bonotto, F., Frey, J., Napoli, M. and Pennathur, S. (2011) Method to Determine the Effective Z Potential in a Microchannel with an Embedded Gate Electrode. *Electrophoresis*, **32**, 3295-3304. https://doi.org/10.1002/elps.201100262

[18] Lu, F., Yang, J. and Kwok, D.Y. (2004) Flow Field Effect on Electric Double Layer during Streaming Potential Measurements. *The Journal of Physical Chemistry B*, **108**, 14970-14975. https://doi.org/10.1021/jp048277z

[19] Chun, M.S., Lee, S.Y. and Yang, S.M. (2003) Estimation of Zeta Potential by Electrokinetic Analysis of Ionic Fluid Flows through a Divergent Microchannel. *Journal of Colloid and Interface Science*, **266**, 120-126. https://doi.org/10.1016/s0021-9797(03)00576-9

[20] Kirby, B.J. and Hasselbrink Jr., E.F. (2004) Zeta Potential of Microfluidic Substrates: 1. Theory, Experimental Techniques, and Effects on Separations. *Electrophoresis*, **25**, 187-202. https://doi.org/10.1002/elps.200305754

[21] He, P., Cheng, L. and Bandaru, P. (2024) Modulation of the Electrokinetic Streaming Potential, as a Function of the Zeta Potential and Fluid Slip. *Chemical Physics Letters*, **834**, Article ID: 140986. https://doi.org/10.1016/j.cplett.2023.140986

[22] Joly, L., Ybert, C., Trizac, E. and Bocquet, L. (2006) Liquid Friction on Charged Surfaces: From Hydrodynamic Slippage to Electrokinetics. *The Journal of Chemical Physics*, **125**, Article ID: 204716. https://doi.org/10.1063/1.2397677

[23] Jing, D. and Bhushan, B. (2013) Effect of Boundary Slip and Surface Charge on the Pressure-Driven Flow. *Journal of Colloid and Interface Science*, **392**, 15-26. https://doi.org/10.1016/j.jcis.2012.09.082

[24] Borges, L.S., Bedin, L. and Bazán, F.S.V. (2021) Multidomain Chebyshev Pseudo-Spectral Method Applied to the Poisson-Boltzmann Equation for Two Parallel Plates. *Journal of Engineering Mathematics*, **127**, Article No. 15. https://doi.org/10.1007/s10665-021-10109-3

[25] Canuto, C., Hussaini, M.Y., Quarteroni, A. and Zang, T.A. (2007) Spectral Methods: Fundamentals in Single Domains. Springer.

[26] Kopriva, D.A. (2009) Implementing Spectral Methods for Partial Differential Equations. Springer.

[27] Baldessari, F. and Santiago, J.G. (2008) Electrokinetics in Nanochannels. Part I: Electric Double Layer Overlap and Channel-to-Well Equilibrium. *Journal of Colloid and Interface Science*, **325**, 526-538. https://doi.org/10.1016/j.jcis.2008.06.007

[28] Baldessari, F. and Santiago, J.G. (2008) Electrokinetics in Nanochannels. Part II: Mobility Dependence on Ion Density and Ionic Current Measurements. *Journal of Colloid and Interface Science*, **325**, 539-546. https://doi.org/10.1016/j.jcis.2008.06.008

[29] van der Heyden, F.H.J., Stein, D. and Dekker, C. (2005) Streaming Currents in a Single Nanofluidic Channel. *Physical Review Letters*, **95**, Article ID: 116104. https://doi.org/10.1103/physrevlett.95.116104

[30] Xie, H., Saito, T. and Hickner, M.A. (2011) Zeta Potential of Ion-Conductive Membranes by Streaming Current Measurements. *Langmuir*, **27**, 4721-4727. https://doi.org/10.1021/la105120f

[31] Chang, C.C. and Yang, R.J. (2009) A Perspective on Streaming Current in Silica Nanofluidic Channels: Poisson-Boltzmann Model versus Poisson-Nernst-Planck Model. *Journal of Colloid and Interface Science*, **339**, 517-520. https://doi.org/10.1016/j.jcis.2009.07.056

[32] Moradmand, A., Saghafian, M. and Moghimi Mofrad, B. (2019) Electroosmotic Pressure-Driven Flow through a Slit Micro-Channel with Electric and Magnetic Transverse Field. *Journal of Applied Fluid Mechanics*, **12**, 961-969. https://doi.org/10.29252/jafm.12.03.28816

[33] Xie, Z., Jian, Y. and Tan, W. (2018) Streaming Potential Analysis and Electrokinetic Energy Conversion Efficiency of Two Immiscible Fluids in a Nanochannel. *Sensors and Actuators B: Chemical*, **273**, 1257-1268. https://doi.org/10.1016/j.snb.2018.06.070

[34] Bernfeld, S.R. and Lakshmikantham, V. (1974) An Introduction to Nonlinear Boundary Value Problems. Academic Press.

[35] Gallardo-Moreno, A.M., Vadillo-Rodríguez, V., Perera-Núñez, J., Bruque, J.M. and González-Martín, M.L. (2012) The Zeta Potential of Extended Dielectrics and Conductors in Terms of Streaming Potential and Streaming Current Measurements. *Physical Chemistry Chemical Physics*, **14**, 9758-9767. https://doi.org/10.1039/c2cp40743d

[36] Peyret, R. (2002) Spectral Methods for Incompressible Viscous Flow. Springer.

[37] Trefethen, L.N. (2000) Spectral Methods in MATLAB. Society for Industrial and Applied Mathematics. https://doi.org/10.1137/1.9780898719598

[38] Björck, Å. (1996) Numerical Methods for Least Squares Problems. Society for Industrial and Applied Mathematics. https://doi.org/10.1137/1.9781611971484

[39] Burden, R.L. and Faires, J.D. (2010) Numerical Analysis. 9th Edition, Cengage Learning.